

Temperature Dependence of Weibull Stress Parameters: Studies Using the Euro-Material Similar to ASME A508 Class-3 Steel

University of Illinois at Urbana-Champaign

**U.S. Nuclear Regulatory Commission
Office of Nuclear Regulatory Research
Washington, DC 20555-0001**



Temperature Dependence of Weibull Stress Parameters: Studies Using the Euro-Material Similar to ASME A508 Class-3 Steel

Manuscript Completed: January 2007
Date Published: March 2007

Prepared by
B. Wasiluk, J.P. Petti and R.H. Dodds, Jr.

Department of Civil and Environmental Engineering
University of Illinois at Urbana-Champaign
205 N. Mathews Avenue
Urbana, IL 61801

S.N.M. Malik, NRC Project Manager

Prepared for
Division of Fuel, Engineering and Radiological Research
Office of Nuclear Regulatory Research
U.S. Nuclear Regulatory Commission
Washington, DC 20555-0001
NRC Job Code Y6951



This page is intentionally blank.

Temperature Dependence of Weibull Stress Parameters: Studies Using the Euro-Material Similar to ASME A508 Class-3 Steel

by

Bogdan Wasiluk, Jason P. Petti, and Robert H. Dodds, Jr.

Abstract

The so-called Beremin model describes the stochastic effects of the cleavage fracture process in ferritic steels at the metallurgical scale. The Beremin model, coupled with large-scale finite element analyses, can be used to understand the effects of constraint loss on the macroscale toughness measured in laboratory test specimens and in full-scale pressure vessels. This process provides the basis for the quantitative *transferability* of fracture toughness measured with a variety of test specimens to structures. The Beremin model leads to a quantity termed the Weibull stress which depends on a number of model parameters. This work demonstrates the temperature invariance of the Weibull stress modulus, m , for a 22NiMoCr37 pressure vessel steel through calibrations at two extreme temperatures of the ductile-to-brittle transition. This temperature invariance reflects the characterization of microcrack size distribution in the material described by the Weibull modulus. The calibrations performed here also demonstrate the clear dependence of the Weibull stress scale parameter, σ_u , on temperature. The increase of σ_u with temperature reflects the increase in microscale toughness of ferritic steels. The calibration procedure employs a three parameter Weibull stress model, which includes the effects of a minimum (threshold) toughness, K_{min} . The calibrations suggest that K_{min} increases gradually with temperature. Finally, an engineering procedure is presented to enable practical applications of the Weibull stress model for defect assessments. This procedure combines the demonstrated temperature invariance of m , a recently developed method for predicting the variation of σ_u with temperature using the ASTM E-1921 Master Curve, and the calibration of the Weibull stress parameters at one temperature. The (calibrated) temperature invariant m and the estimated σ_u as a function of temperature are used to predict the cumulative probability of fracture for several large datasets without direct calibration.

This page is intentionally blank.

Foreword

Appendix G, “Fracture Toughness Requirements,” to Part 50 of Title 10 of the Code of Federal Regulations (10 CFR Part 50), “Domestic Licensing of Production and Utilization Facilities,” specifies fracture toughness requirements for ferritic materials of pressure-retaining components of the reactor coolant pressure boundary of light-water nuclear power reactors. These requirements provide reasonable assurance that adequate margins of safety are maintained during any condition of normal operation, including anticipated operational occurrences, to which the pressure boundary may be subjected over its service lifetime. Similarly, the Pressurized Thermal Shock Rule (10 CFR 50.61) describes fracture toughness requirements for protection against brittle fracture that could occur as a result of pressurized thermal shock events. Over the past 5 years, several licensees have requested changes to their licensing bases through application of master curve (MC) technology for fracture toughness characterization, as codified by the American Society for Testing and Materials (ASTM) in ASTM E-1921, “Standard Test Method for Determination of Reference Temperature, T_0 , for Ferritic Steels in the Transition Range.” Such uses of MC technology by the industry can be expected to continue until the Nuclear Regulatory Commission (NRC) revises both the Pressurized Thermal Shock Rule and the heatup and cooldown limits associated with Appendix G to 10 CFR Part 50. The MC relies on an elastic-plastic characterization of fracture toughness, while the current regulatory framework is based wholly on linear-elastic fracture mechanics (LEFM) calculations. The NRC has reviewed these license amendment requests employing conservative adjustments to accommodate elastic-plastic fracture mechanics (EPFM) analytical results in the LEFM regulatory framework. If an EPFM-based probabilistic fracture mechanics tool were available, these safety evaluations of RPVs could be performed in an equally technically rigorous, but more efficient and less conservative manner.

This report addresses the appropriate application (for certain types of loading scenarios) of EPFM material toughness parameters measured using laboratory specimens to the evaluation of defects in large structures. The present work describes a novel approach that couples a Weibull stress model to characterize cleavage fracture processes, with the well-understood and validated MC statistical model. The approach employs the massive data set of fracture toughness generated recently in Europe for a common RPV steel, combined with high-fidelity, nonlinear, three-dimensional computational analyses of test specimens. The resulting observations reflect the temperature-independence of a key Weibull stress parameter over the ductile-to-brittle transition region, in addition to the temperature-dependence of the Weibull scale parameter, at least for this important steel. This work represents a significant step in the development and application of an EPFM-based probabilistic fracture mechanics tool.

Brian W. Sheron, Director
Office of Nuclear Regulatory Research
U.S. Nuclear Regulatory Commission

This page is intentionally blank.

Contents

Abstract	iii
Foreword	v
Contents	vii
Figures	ix
Tables	xi
Acronyms	xiii
Executive Summary	xv
Acknowledgements	xvii
1. Introduction.....	1
2. Modeling of Cleavage Fracture Toughness	5
2.1 Weakest Link Model	5
2.2 The Weibull Stress Model.....	6
2.3 Summary of Weibull Stress Parameters.....	9
3. Calibration of the Weibull Stress Model.....	11
4. Finite Element Modeling.....	15
5. Results from Calibration Procedure.....	17
5.1 European Program.....	17
5.2 Calibration Strategy.....	18
5.3 Calibration at -40°C	18
5.4 Calibration at -110°C	19
5.5 Consequences of Temperature Invariant m -Value	20
6. Predictions Over Full DBT by Coupling with the Master Curve.....	23
7. Summary and Conclusions.....	27
References.....	29
Appendix: Calibration Error Measures	31

This page is intentionally blank.

Figures

1.	Weibull stress values and constraint correction g-functions computed using stress-strain properties for the Euro material at -40°C . Weibull stress modulus taken as $m = 10$ for these illustrative results.	33
2.	Quasi-static, uniaxial stress-strain curves for Euro-program material (22NiMoCr37 pressure vessel steel). (a) true stress-logarithmic strain curves over a range of temperatures in the DBT region; and (b) yield stresses measured over the DBT region.....	34
3.	One-quarter symmetric finite element models for (a) C(T) specimen with $a/W = 0.56$, (b) pre-cracked, 0.4T Charpy V-Notch specimen with $a/W = 0.56$, and (c) small-scale yielding (SSY). All models have finite root radius along crack front.	35
4.	Cumulative (rank) fracture probabilities of raw experimental datasets for the Euro material at (a) $T = -40^{\circ}\text{C}$, (b) $T = -110^{\circ}\text{C}$, (c) $T = -20^{\circ}\text{C}$. These data drive the calibration process for the Weibull stress parameters. The reference temperature $T_0 = -90^{\circ}\text{C}$ from C(T) specimens.....	36
5.	Cumulative (rank) fracture probabilities of raw experimental datasets for the Euro material at (a) $T = -91^{\circ}\text{C}$, (b) $T = -60^{\circ}\text{C}$, (c) $T = -110^{\circ}\text{C}$. These data drive checking of the Weibull stress parameters calibrated using other datasets. The reference temperature $T_0 = -90^{\circ}\text{C}$ from C(T) specimens.....	37
6.	Cumulative (rank) fracture probabilities of experimental datasets for the Euro-material crack-front length adjusted to 1T using E1921 procedure at (a) $T = -40^{\circ}\text{C}$, (b) $T = -110^{\circ}\text{C}$, (c) $T = -20^{\circ}\text{C}$. The reference temperature $T_0 = -90^{\circ}\text{C}$ from C(T) specimens.	38
7.	Calibration of Weibull stress parameters for the Euro-material at $T = -40^{\circ}\text{C}$ and $T = -110^{\circ}\text{C}$ Normalized values of error function over range of m -values (a,c); corresponding K_{min} values that lead to minimum error values for each m -value.	39
8.	Correction of Euro-material datasets to 1T SSY condition at $T = -40^{\circ}\text{C}$ and $T = -110^{\circ}\text{C}$. Using calibrated values of (m, K_{min}) in (a,c); using other values of (m, K_{min}) to illustrate errors of using non-calibrated values.	40
9.	Predicted fracture probabilities of Euro-material using calibrated Weibull stress parameters: (a) $T = -40^{\circ}\text{C}$ data used in calibration, (b) $T = -110^{\circ}\text{C}$ data used in calibration and (c) $T = -40^{\circ}\text{C}$ data not used in calibration.....	41
10.	Predicted fracture probabilities for Euro-material specimens not used in any calibrations. Weibull modulus fixed at $m = 20$, $K_{min} = 20 \text{ MPa}\sqrt{\text{m}}$ with temperature dependent σ_u based on the Master Curve. (a) $T = -91^{\circ}\text{C}$, (b) $T = -60^{\circ}\text{C}$, (c) $T = -20^{\circ}\text{C}$ and (d) $T = -110^{\circ}\text{C}$	42
A1.	Illustration of contributions to the error measure for calibration of the Weibull stress parameters. (a) difference between experimental data scaled to 1T SSY and	

calculated failure probability using 3-parameter form of E1921; (b) difference between
low and high constraint experimental data scaled to 1T SSY..... 43

Tables

1. Characteristic parameters of three parameter Weibull stress model for the Euro-material.....	44
---	----

This page is intentionally blank.

Acronyms

DBT = ductile-to-brittle transition

SSY = small-scale yielding

SE(B) = single-edge notched bend specimen

C(T) = compact tension specimen

CVN = Charpy V-Notch specimen

HC = high constraint

LC = low constraint

ASME = American Society of Mechanical Engineers

ASTM = American Society for Testing and Materials

This page is intentionally blank.

Executive Summary

This work advances the understanding and applicability of numerical models to predict the cleavage fracture process in structural components fabricated from ferritic steels and operated over the ductile-to-brittle transition (DBT) region of temperatures. The pressure vessels of commercial nuclear power plants are fabricated from the ferritic steels of specific interest in this study. Significant research programs have recently been completed to characterize the ductile-to-brittle transition behavior of ferritic steels. This behavior proves challenging to quantify given the shift in (metallurgical scale) fracture mechanism from void growth and coalescence to transgranular cleavage as the temperature decreases. The potential for cleavage fracture causes concern since sudden failure can occur by cleavage without extensive prior deformation. The necessity for probabilistic failure assessment evolves naturally from the large statistical scatter observed in measured toughness values in the DBT regime. The scatter reflects a “weakest link” phenomenon where one or more initiation sites at metallurgical-scale inclusions trigger sudden fracture of a test specimen or structure. The observed scatter shows a strong sensitivity to the volume of material at the crack front subjected to high stresses and leads to the also observed strong variations of toughness across specimen geometry, *e.g.*, shallow-notch SE(B)s compared to conventional C(T)s, for examples see [8].

The DBT behavior of ferritic steels has been studied widely, leading to engineering approaches that characterize the scatter and temperature dependence of macroscopic fracture toughness values. The ASTM E1921 [1] testing standard quantifies the DBT behavior of ferritic steels. The standard employs a three parameter Weibull distribution for the cumulative probability of cleavage fracture at each temperature over the DBT. E1921 also utilizes the empirically based “Master Curve” to estimate the temperature-toughness relationship over the DBT for a wide range of ferritic steels. The Master Curve concept defines the relationship between the median fracture toughness K_{Jc} ($P_f = 0.5$) for high constraint conditions and the normalized temperature, $T-T_0$, for a 1T size specimen. Once T_0 becomes known for a specific material, un-normalization of the Master Curve produces an estimate of the median toughness throughout the DBT.

The assumption that small-scale yielding (SSY) conditions exist at fracture limits the usefulness and application of the testing standard in practice. Alternative methods, including the Beremin model [6], have found widespread use and development to address the cleavage modeling at the metallurgical scale. The Beremin model introduces a statistical treatment for the distribution of fracture initiators (*e.g.*, microcracks formed at inclusions) to develop a probabilistic approach for cleavage fracture. The Beremin model defines the scalar, microstructural fracture parameter, the so-called Weibull-stress (σ_w), which reflects the random distribution of microcracks at the crack front. The model includes two parameters, the Weibull modulus (m) and the Weibull scale parameter (σ_u). The Weibull modulus, m , characterizes the size distribution of microcracks, while the Weibull scale parameter, σ_u , represents the aggregate microcrack toughness [6]. In the Weibull stress framework, these two parameters describe material features invariant of crack-front constraint, crack-front length, etc.

Over the past twenty years, several different methods have evolved to calibrate the Weibull stress parameters. Gao et al. [8] and Ruggieri et al. [12,13] show that non-unique calibrations are produced with early calibration methods based entirely on deep-notch toughness values. Petti and Dodds [14] went on to suggest coupling the Master Curve description of the macroscale toughness-temperature relationship with the calibration procedure to set the Weibull scale parameter, σ_u . This method produces an estimate of σ_u as a function of temperature for the material throughout the DBT with a direct calibration at only one temperature, most likely the testing temperature adopted to establish T_0 .

Starting from the recent work by Petti and Dodds [14], the present study utilizes the extensive datasets generated during a recent Euro-testing program on a reactor pressure vessel steel to explore the temperature dependence of the Weibull stress modulus, m . Calibrations described here at two widely different temperatures demonstrate the temperature independence of m over the DBT region, in addition to the

temperature dependence of the Weibull scale parameter, σ_u . Applications of this engineering procedure to several datasets for the Euro-material, not included in calibrations, show excellent predictions and demonstrate significant promise for this method.

Acknowledgements

This investigation was supported by grants principally from the U.S. Nuclear Regulatory Commission, Office of Regulatory Research and from the Naval Surface Warfare Center, Carderock Division. Additional financial support was provided by the M.T. Geoffrey Yeh Endowed Chair Fund in the Department of Civil & Environmental Engineering at the University of Illinois. We wish to acknowledge the many valuable discussions and data contributions from Dr. Kim Wallin, VTT (Finland) and Dr. Juergen Heerens, Institut für Werkstofforschung (GKSS Forschungszentrum).

This page is intentionally blank.

1 Introduction

Significant research programs have recently been completed to characterize the ductile-to-brittle transition (DBT) behavior of ferritic steels. This behavior proves difficult to assess with the shift in fracture mechanism from void growth and coalescence to transgranular cleavage as the temperature decreases throughout the DBT region. The potential for cleavage fracture causes concern since sudden failure can occur by cleavage without extensive prior deformation. Complications in failure assessments also stem from the large scatter observed in measured toughness values in the DBT regime. The scatter reflects a “weakest link” phenomenon where one or more initiation sites at metallurgical-scale inclusions trigger sudden fracture of the specimen-structure. The observed scatter shows a strong sensitivity to the volume of material at the crack front subjected to high stresses and leads to the also observed strong variations of toughness across specimen geometry, *e.g.*, shallow-notch SE(B)s compared to conventional C(T)s, for examples see [8].

The DBT behavior of ferritic steels has been studied widely, leading to engineering approaches that characterize the scatter and temperature dependence of macroscopic fracture toughness values. The ASTM E1921 [1] testing standard quantifies the DBT behavior of ferritic steels. The standard employs a three parameter Weibull distribution for the cumulative probability of cleavage fracture at each temperature over the DBT. The distribution maintains a constant exponent of 4 to reflect the requirement that small-scale yielding (SSY) conditions exist at fracture in each specimen. The Weibull distribution also includes a minimum (threshold) toughness, K_{min} , to enforce the experimental observation that the probability of fracture remains zero below a small, but finite toughness value. E1921 also utilizes the empirically based Master Curve to estimate the temperature-toughness relationship over the DBT for a wide range of ferritic steels. The Master Curve concept developed by Wallin [2,3,4,5] defines the relationship between the median fracture toughness K_{Jc} ($P_f = 0.5$) for high constraint conditions and the normalized temperature, $T - T_0$, for a 1T size specimen. The reference temperature, T_0 , defines the temperature at which the median fracture toughness for a 1T crack-front length equals $100\text{MPa}\sqrt{\text{m}}$. Once T_0 becomes known for a specific material, un-normalization of the Master Curve produces an estimate of the median toughness throughout the DBT. Simple weakest link models enable adjustment of non-1T size fracture toughness values for use with the Master Curve provided the SSY conditions exist.

The assumption that small-scale yielding (SSY) conditions exist at fracture limits the usefulness and application of the testing standard for situations when high constraint conditions do not exist at fracture, *e.g.*, large deformation prior to fracture in higher toughness materials or in naturally low constraint specimens and structures (those with T -stress < 0). Since the simple weakest link model for the macro-scale toughness fails to remain applicable under these conditions, alternative methods, including the Beremin model [6], have found widespread use and development. The Beremin model introduces a statistical treatment for the distribution of fracture initiators (*e.g.*, microcracks formed at inclusions) to develop a probabilistic approach for cleavage fracture. The Beremin model defines the scalar, microstructural fracture parameter, the so-called Weibull-stress (σ_w), which reflects the random distribution of microcracks at the crack front. The model includes two parameters, the Weibull modulus (m) and the

Weibull scale parameter (σ_u). The Weibull modulus, m , characterizes the size distribution of microcracks, while the Weibull scale parameter, σ_u , represents the aggregate microcrack toughness [6]. In the Weibull stress framework, these two parameters describe material features invariant of crack-front constraint, crack-front length, etc.

Bakker and Koers [7] proposed an important extension of the original Beremin model by introducing a threshold stress, σ_{th} , to incorporate the existence of experimentally observed threshold toughness values. In their proposal, cleavage fracture becomes possible only when the critical stress acting on the volume surrounding a microcrack exceeds a specific, material threshold value. Measurement or estimation of σ_{th} becomes problematic and affects strongly the calibration of Weibull stress parameters (m, σ_u). Gao *et al.* [8] suggest an alternate approach, which introduces a minimum Weibull stress, σ_{w-min} . This simplifies considerably the introduction of a threshold toughness since σ_{w-min} is taken as the value of σ_w at a given minimum macroscopic fracture toughness, K_{min} . More recently, Kroon and Faleskog [9,10], among others, include the effects of plastic strain in a Weibull stress framework to reflect additional microcrack nucleation under loading. These extensions of the original Beremin model continue to advance its usefulness and practical application.

Over the past twenty years, several different methods have evolved to calibrate the Weibull parameters. Minami *et al.* [11] and Bakker and Koers [7] use one set of fracture toughness values obtained from a high constraint geometry. Minami *et al.* [11] describe a maximum likelihood method which employs statistical estimators (α, β) to enforce equal probability distributions between the macroscopic and microscopic parameters, $(J_c/\beta)\alpha=(\sigma_w/\sigma_u)m$. Gao *et al.* [8] and Ruggieri *et al.* [12,13] show that non-unique calibrations are produced with this method since two parameters (m, σ_u) are calibrated with experimental data having crack-front fields at fracture controlled by a single loading parameter (J). They also showed that use of test specimens with widely differing constraint levels does lead to a unique calibration. Recent work by Petti and Dodds [14] argues that the Weibull modulus, m , may be independent of temperature in the DBT region, while the Weibull scale parameter, σ_u , increases with temperature. If this holds, calibrations would still appear to be required at every temperature of interest over the DBT region. To overcome this severe limitation, Petti and Dodds [14] suggest coupling the Master Curve description of the macro-scale toughness-temperature relationship with the calibration procedure to set the Weibull scale parameter, σ_u . This method produces an estimate of σ_u as a function of temperature for the material throughout the DBT with a direct calibration at only one temperature, most likely the testing temperature adopted to establish T_0 . There does not appear to exist a “Master Curve” for ferritic steels in terms of parameters (m, σ_u) since these parameters, for the limited set of materials calibrated to date, vary significantly.

Recently, Wallin [15] applied the E1921 procedures to the extensive datasets produced in a European Union project [16] entitled “Fracture toughness of steel in the ductile-to-brittle transition regime.” This project thoroughly characterized the behavior of a quenched-and-tempered pressure vessel steel, DIN 22NiMoCr37 (similar to the American A508 C1.3 steel). More than 800 tests were performed using compact tension (C(T)) specimens ranging in size from 0.5T to 4T with test temperatures spanning the entire DBT. Follow-on work by Heerens *et al.* [17], among others, tested over 400 pre-cracked Charpy (CVN) specimens extracted from the broken larger specimens. These very large datasets validate the statistical

and Master Curve concepts-procedures adopted in E1921 and provide invaluable datasets for validation of micromechanical models such as described in this study.

Starting from the recent work by Petti and Dodds [14], the present study utilizes the extensive datasets from the Euro-testing program to explore the temperature dependence of the Weibull stress modulus, m . Calibrations described here at two widely different temperatures demonstrate clearly the temperature independence of m over the DBT region, in addition to the temperature dependence of the Weibull scale parameter, σ_u . The calibration procedure adopted here also examines “best fit” values for the threshold toughness, K_{min} . Finally, we describe examples of the procedure that demonstrate practical use of the Weibull stress model for engineering applications in defect assessments. The procedure requires calibration of the Weibull parameters at only one temperature and knowledge of the reference temperature, T_0 , for the material. The procedure assumes m remains invariant of temperature and uses a modified version of the method introduced by Petti and Dodds [14] to estimate σ_u at temperatures throughout the DBT without direct calibration through use of the Master Curve. As would be followed in practice, K_{min} is fixed in this demonstration example at the E1921 recommended value of $20 \text{ MPa}\sqrt{\text{m}}$. Applications of this engineering procedure to several datasets for the Euro-material, not included in calibrations, show excellent predictions and demonstrate significant promise for this method.

The organization of this report is as follows. Section 2 reviews the modeling of cleavage fracture including both the weakest link-based model and Weibull stress framework. Section 3 presents an improved calibration procedure for the three-parameter Weibull stress model. Section 4 describes the finite element models and computational procedures. Section 5 discusses the European testing program and the calibration of the Euro-material at two temperatures, -110°C and -40°C . Section 6 employs the Master Curve to perform multi-temperature predictions throughout the DBT region. Finally, Section 7 summarizes the conclusions supported by this study.

This page is intentionally blank.

2 Modeling of Cleavage Fracture

2.1 Weakest Link–Based Model

Weakest link concepts form the technical basis for the first testing standard developed specifically to address the unique statistical issues with ferritic steels in the ductile-to-brittle transition region (ASTM E1921 [1]). As expressed in E1921, the weakest-link model requires that the local stress field and J -values remain essentially uniform along the entire crack front and that small-scale yielding (SSY) conditions prevail at the cleavage fracture event. This greatly simplifies description of the crack-front loading but limits the application of such approaches to fracture specimens (and structures) prior to the development of significant constraint loss under increased plastic deformation. Under SSY conditions, the crack driving force may be expressed for convenience in terms of a K_J -value, *i.e.*, $K_J = \sqrt{EJ/(1-\nu^2)}$.

Based on these assumptions, the three-parameter statistical model employed in E1921 adopts a constant exponent (modulus) of four in the Weibull expression for the cumulative fracture probability at each temperature over the ductile-to-brittle transition,

$$P_f(K_{Jc}) = 1 - \exp\left[-\left(\frac{K_{Jc} - K_{min}}{K_0 - K_{min}}\right)^4\right], \quad (1)$$

where K_{min} denotes the minimum fracture toughness, $P_f(K_{Jc} \leq K_{min}) = 0$. E1921 sets K_{min} equal to 20 MPa√m, invariant of material flow properties, crack-front configuration, and temperature. The temperature dependent K_0 -value corresponds to the fracture toughness when the cumulative probability of failure equals 63.2%, $P_f(K_{Jc} = K_0) = 0.632$. The maximum likelihood method provides the estimate for K_0 from measured toughness values as,

$$K_0 = \left[\sum_{i=1}^N \frac{(K_{Jc(i)} - K_{min})^4}{(r - 0.3068)} \right]^{1/4} + K_{min}, \quad (2)$$

where N and r denote the total number specimens in a dataset and the number of uncensored (valid) values, respectively. The E1921 procedures censor measured values of fracture toughness that violate SSY conditions; toughness values have a limiting value of K_{Jc} given by,

$$K_{Jc} \leq \sqrt{\frac{Eb\sigma_0}{M_{limit}(1-\nu^2)}}, \quad (3)$$

where b , E , ν , and σ_0 denote the remaining ligament, Young's modulus, Poisson's ratio, and yield stress. E1921 currently adopts a value of 30 for the limiting, non-dimensional deformation, M_{limit} ; a value now widely accepted as applicable for standard, deep-notched compact tension specimens, C(T)s.

Toughness values measured using fracture specimens tested at other (xT) than 1T thickness (crack-front length of 25.4 mm), require a statistical adjustment to an equivalent 1T value for comparisons. The

E1921 requirement for a uniform J -value along the front and for SSY conditions makes the adjustment process straightforward. The highly stressed volume of material along the crack front then scales with $B \times K_J^4$ and thus equivalent P_f values for different crack-front lengths through Eq. (1) require that

$$K_{Jc}^{E1921(IT)} = K_{min}^{E1921} + \left(K_{Jc}^{(\alpha T)} - K_{min}^{E1921} \right) \left(\frac{B_{\alpha T}}{B_{IT}} \right)^{1/4}, \quad (4)$$

where $K_{min}^{E1921} = 20 \text{ MPa}\sqrt{\text{m}}$ and B denotes specimen thickness.

2.2 The Weibull Stress Model

The *macroscopic* fracture model represented by Eqs. (1, 4) applies under conditions of high-constraint (T -stress ≥ 0), SSY when each crack front location has the same applied J -value. SSY conditions insure the unique correspondence across specimens between the crack-front J -value and the local crack-front strains-stresses at fracture. The corresponding *microscopic* fracture model employs directly the strain-stresses at each crack-front location; SSY conditions then become unnecessary to establish the link with the scalar measure (J) of the loading. The Beremin group [6] introduced the most widely used and developed microscopic model. In this model, a local fracture parameter, the so-called Weibull stress (σ_w), defines a scalar measure of the crack-front conditions driving cleavage fracture at increasing levels of external loading. Numerical analyses connect values of σ_w with external loading of the specimen-structure and may include complexities from variable crack-front geometry, large-scale yielding, thermo-mechanical loading, etc. In its original form, σ_w describes the crack-front loading in a two-parameter Weibull expression for the cumulative fracture probability [6] follows as,

$$P_f(\sigma_w) = 1 - \exp \left[- \left(\frac{\sigma_w}{\sigma_u} \right)^m \right], \quad (5)$$

where the scalar Weibull stress, σ_w , is given by,

$$\sigma_w = \left[\frac{1}{V_0} \int_V \sigma_1^m dV \right]^{1/m}. \quad (6)$$

where V denotes the highly-stressed volume of material just ahead of the crack front over which the triggering event of cleavage fracture occurs. The Beremin group showed the link between the Weibull modulus, m , and the postulated shape of the probability density function for pre-existing microcracks that form at metallurgical- scale inclusions, at grain boundaries, etc. The value of m quantifies the degree of “scatter” reflected in the cumulative failure probability distribution, analogous to the “4” exponent in the macroscopic model of Eq. (1). The Weibull-stress scale parameter, σ_u , denotes the Weibull stress value for a cumulative probability of fracture equal to 0.632, $P_f(\sigma_w = \sigma_u) = 0.632$. The Weibull stress is computed most often by integrating the maximum principal stress, σ_1 , over the fracture process zone, V , at each stage of loading. This zone consists of the region of plastically deformed, crack-front material over which the maximum principal stress exceeds a multiple (λ) of the yield stress $\sigma_1 \geq \lambda \sigma_0$. Petti and Dodds [18] illustrate that the specified value for λ does not affect the calibrated values of m for smaller m -values

≤ 10 to 12, but not the relative toughness values between differing crack-front conditions. Here we employ the common value of 2 for λ . The normalizing volume, V_0 , cancels in applications of the Weibull stress model to compare crack-front conditions for the same material and is assigned a value here of unity.

Under strict plane-strain and SSY conditions, the macroscopic and microscopic fracture models have a unique and the now well-understood connection [6,8],

$$\sigma_w^m = C B J^2 \text{ or } \sigma_w^m = \bar{C} B K_J^4, \quad (7)$$

where C and $\bar{C} = C \left[(1-\nu^2) / E \right]^2$ denote a material constant dependent on the material flow properties at the temperature of interest and on Weibull stress parameters (m, V_0).

Actual fracture specimens eventually violate SSY conditions to varying degrees with increasing load. Gao and Dodds [19] modified Eq. (7) by inserting a non-dimensional constraint function, $g(M)$. The g -function characterizes the level of constraint difference between the ideal, plane-strain SSY conditions (with T -stress = 0) and a specific fracture specimen,

$$\sigma_w^m = C B J_{avg}^2 g(M) \text{ or } \sigma_w^m = \bar{C} B K_{J(avg)}^4 g(M), \quad (8)$$

Where $M = b \sigma_0 / J_{avg}$ and J_{avg} denotes a through-thickness average value. The constraint function, $g(M)$, equals 1.0 for all materials under plane-strain, SSY conditions with T -stress = 0. For a specific configuration, 3-D nonlinear finite element analyses and Weibull stress computations produce σ_w vs. J_{avg} values. A plane-strain, SSY boundary-layer analysis with T -stress = 0 readily yields the constant C for a specific material and m value (see [8] for examples). The g -function value (with respect to M) then follows by solving Eq. (8) for $g(M)$ at each loading level in the specimen--structure. As SSY conditions degenerate along the crack-front under increased loading, the $g(M)$ -values gradually fall below the 1.0 level. By expressing g -functions in terms of the non-dimensional deformation, M , the $g(M)$ function for a material remains invariant for all geometrically similar specimens, *e.g.*, all SE(B)s for the material at the specified temperature with $a/W = 0.5$, $B \times B$ cross-section and span = $4W$ have the same $g(M)$ invariant of the specific thickness B .

Figure 1 illustrates the Weibull stress values for the SSY reference condition and for plane-sided C(T) specimens computed using the stress-strain properties for the Euro material at -40°C . Figure 1a compares the Weibull stress values (normalized by the yield stress at -40°C) with increased loading for 1T SSY and 1T C(T) configurations using a representative Weibull stress modulus of $m=10$. The 1T SSY values enable computation of the material constant C appearing in Eq. (7). Figure 1b recasts the same results with the loading normalized in terms of the non-dimensional deformation parameter, M , where J -values for SSY are normalized using b for the C(T) specimen. Figure 1c shows the constraint function, $g(M)$, for the C(T) specimen computed directly from the curves in Fig. 1b through Eq. (8) and the material constant C . Differences between the 1T SSY, which have $g(M) \equiv 1.0$, and 1T C(T) curves reflect the levels of constraint loss in the C(T) specimen under increasing load. Figure 1c also reveals the strongly positive T -stress in the C(T) specimen at large M -values where $g(M)$ exceeds 1.0. Figures 1(a-c) illustrate clearly the very gradual constraint loss, which makes difficult the specification of a “single” limiting M -value for specimens in testing standards. Recall also that the $m=10$ used in these illustrative results influ-

ences the constraint loss - calibrated m -values larger than 10 would reduce the differences between the SSY and C(T) curves. Compared to the strict plane-strain, SSY reference condition, the C(T) specimen begins to lose constraint ($g(M)$) when $M \approx 300$ (based on $m = 10$). The value $g(M) = 0.5$, for example, implies a 16% difference in K_J -values between C(T) and SSY conditions at the same Weibull stress value, and thus the same fracture probability. Figure 1d shows the effect of specimen size on the Weibull stress values for the C(T) specimen. The C(T) curves reflect the coupled effects of absolute crack front length (statistical) and constraint loss (deterministic) for increasing J -values. However, each of these proportionally scaled C(T) specimens has the identical g -function curve shown in Fig. 1c.

By adopting the three-parameter form for the cumulative fracture probability in Eq. (1), E1921 assumes high-constraint, SSY conditions exist at fracture and includes threshold toughness. Extension of the Weibull stress model to match the E1921 characterization of toughness scatter at each temperature requires threshold toughness in a three-parameter cumulative probability of fracture [18]. Gao and Dodds [19] and Petti and Dodds [14,18] modified the Weibull stress model to include constraint loss, crack-front length effects, and a minimum Weibull stress value to predict a minimum (threshold) toughness,

$$P_f(\sigma_w) = 1 - \exp \left[- \left(\frac{\sigma_w^{m/4} - \sigma_{w-min}^{m/4}}{\sigma_u^{m/4} - \sigma_{w-min}^{m/4}} \right)^4 \right] \text{ for } \sigma_w > \sigma_{w-min}, \quad (9)$$

$$P_f(\sigma_w) = 0 \text{ for } \sigma_w \leq \sigma_{w-min} \quad (10)$$

The minimum (threshold) Weibull stress, $\sigma_{w-min} [\sigma_{w-min} = \sigma_w (K_J = K_{min})]$, depends on the crack-front length, material flow properties, and the Weibull parameters (m, ν_0). For plane strain SSY conditions, Petti and Dodds [18] showed that the specific three-parameter form above leads to identical scaling of crack-front length effects on the fracture toughness using the Weibull stress model (for all m -values) and the E1921 expression, Eq. (4).

In the two-parameter Weibull stress model, Eq. (5), the denominator within the exponential (σ_u) remains invariant of changes in crack-front length and constraint level for a constant temperature and loading rate, *i.e.*, σ_u represents a material property. The three-parameter expression in Eq. (9) introduces a σ_{w-min} in the denominator. But because σ_{w-min} varies with crack-front length and (potentially) constraint, σ_u must now change to maintain a constant denominator for all crack-front lengths and (potentially) different constraint levels [14]. In practice, the small differences in constraint levels between identical thickness, deep-notch SE(B) specimens, C(T) specimens, and the plane-strain SSY (T -stress = 0) reference condition when $K_{min} \leq 20 \text{ MPa}\sqrt{\text{m}}$ lead to a negligible effect on σ_u .

By using the three-parameter expression in Eq. (9), a ‘‘toughness scaling’’ model arises which converts measured toughness values for xT size specimens (including constraint loss) to 1T plane-strain SSY conditions [18]. Written as an extension of Eq. (4), the toughness scaling model has the form

$$K_{Jc}^{SSY(1T)} = K_{min} + \left[g(M^{(xT)})^{1/4} K_{Jc}^{(xT)} - g(M_{min}^{(xT)})^{1/4} K_{min} \right] \left(\frac{B_{xT}}{B_{1T}} \right)^{1/4}, \quad (11)$$

where $g(M_{min}^{(xT)} \neq 1.0)$, with $M_{min}^{(xT)} = b_{xT} \sigma_0 E / \left[(1 - \nu^2) K_{min}^2 \right]$, for low constraint specimens and for high constraint specimens when $K_{min} \geq 20 \text{MPa}\sqrt{\text{m}}$ [18]. For common test specimen sizes (1T), no constraint loss occurs at the applied loading of $K = K_{min}$ and the above expression simplifies with $g(M_{min}^{(xT)} \neq 1.0)$. The $g(M)$ function varies with temperature and loading rate due to the change in material flow properties. This approach also applies equally for a different selection of the “reference” condition. For example, ongoing work of the E1921 committee envisions use of a 1T C(T) specimen as the reference condition rather than the more stringent 1T, plane-strain SSY (T -stress = 0) condition.

2.3 Summary of Weibull Stress Parameters

At the *macroscale*, the cleavage fracture toughness under SSY conditions is taken here to be described by the approach in ASTM E-1921. At each temperature in the DBT region, the statistical distribution of measured fracture toughness values is represented by Eq. (1). The macroscale parameters are: (1) the fixed exponent of 4 (taken as invariant of temperature), (2) the median fracture toughness, K_0 , which varies with temperature and crack front length, and (3) the threshold toughness K_{min} below which the fracture probability vanishes (taken as temperature and crack-front length invariant in E-1921). The fixed exponent of 4 derives from the (strict) conditions of SSY under which the “in-plane” plastic zone size increases in area proportional to K_J^4 (invariant of temperature). The volume of crack front plastic zone thus increases proportional with crack front length (*i.e.*, B) $\times K^4$. In Eq. (1), the probability of cleavage fracture thus varies in proportion to the volume of highly stressed material containing metallurgical triggering points along the crack front. In this work, we use the extensive experience with large-scale fracture testing programs conducted over the past 10+ years framed in terms of the E-1921 approach. Under SSY conditions, a calibrated implementation of the Weibull stress model must predict the toughness-temperature variation of E-1921 and the statistical distribution of K_{Jc} values at each temperature described by Eq. (1).

In the Weibull stress microscale model, the exponent (m) is coupled to an *assumed*, inverse power law description for the probability density function of initiating sites for cleavage fracture. Because the exponent reflects the statistical distribution of pre-existing trigger points for cleavage fracture, it is argued to be temperature and constraint invariant. The temperature dependence appears in the toughness scale parameters, σ_u , analogous to the temperature dependent K_0 value in Eq. (1). Petti and Dodds [14] re-examine the fundamental assumptions of the Weibull stress model and argue that σ_u reflects the microscale toughness (F_c) of material that encloses metallurgical scale cracks and thus varies with temperature. The temperature dependence of the material flow stress enters into σ_u as well but is a clear second-order effect. As a “local,” metallurgical-scale parameter, σ_u is assumed to not vary with constraint, since it reflects the actual stress computed to act upon a local material volume that drives the Weibull stress model, not the stress *inferred* to exist on the assumption that SSY conditions exist with stress field amplitude governed by K_J .

The simplest, two-parameter Weibull stress model does not predict a threshold value of macroscopic toughness. This contradicts directly the E-1921 description of toughness which has the threshold toughness, K_{min} . Ruggieri, *et. al.* [13] suggest using K_{min} to define a threshold value of the Weibull stress, σ_{w-min}

= $\sigma_w (K_J = K_{min})$, together with the 3-parameter form in Eq. (9), which enables prediction of the E-1921 statistical distribution, Eq. (1), when SSY conditions do exist. Because the material flow properties vary with temperature, σ_u likewise varies with temperature and crack front length for a fixed K_{min} .

3 Calibration of the Weibull Stress Model

The values of fracture toughness predicted using the Weibull stress model depend strongly on the calibrated values of the Weibull stress parameters (m, σ_u). Gao *et al.* [8, 20] and Ruggieri *et al.* [13] first demonstrated the source of difficulties in earlier calibration procedures which employ a single set of high-constraint toughness values, with crack-front fields characterized by only J , to calibrate the two parameters. They introduced a new calibration procedure, which leads to unique sets of calibrated parameters. This procedure utilizes the constraint differences between two different sets of measured fracture toughness values - one set measured using high constraint specimens and one set measured using low constraint specimens. The low constraint specimens fracture at crack-front conditions characterized by at least two independent parameters (*i.e.*, J and the T -stress or the Q -stress), which enables calibration for a unique pair (m, σ_u). The method proceeds by using trial values of m to constraint correct (scale) each set of toughness values to a common reference configuration (most often plane-strain, SSY with zero T -stress). The calibrated pair of Weibull parameters (m and then σ_u) best collapses the two experimental data sets to the same distribution of cumulative fracture probability when scaled to the reference condition.

For three-parameter models such as Eq. (9), additional procedures must be introduced to calibrate the third-parameter, K_{min} (or σ_{w-min}). Petti and Dodds [14,18] employ a simple least squares procedure in combination with constraint correction to calibrate all three-parameters. They assign equal weight to all measured toughness values in the calibration process. This method not only produces similar toughness distributions for the high and low constraint data sets when scaled to a common reference condition, but finds the set of parameters that produce a “best-fit” of Eq. (9) to the experimental data. In earlier work [8,13,20], the simple calibration procedure forced equivalence of only K_0 -values for the two scaled distributions, which often led to less than satisfactory fits for toughness values at low and high fracture probabilities. Here, we employ an updated version of the least squares procedure. This error function applies a weight factor to each measured toughness value designed to reduce the relative contribution of experimental values that differ the greatest amount from the mean of the measured values. The Appendix provides a detailed description of the error measure.

The following steps describe the calibration procedure:

1. *Test two sets of specimens at the same temperature in the DBT region that have markedly different constraint:*
 - *high constraint (HC) data set, with n_{HC} specimens, that approaches small-scale yielding conditions, having $M \geq 100$*
 - *a low constraint (LC) data set, with n_{LC} specimens, under large-scale yielding but without significant ductile tearing prior to cleavage fracture in each specimen*

The subsequently calibrated parameters for the Weibull stress model then apply strictly for the test temperature.

2. *Obtain uniaxial, (true) stress-strain curve for the test temperature to strain values of ≈ 2.0 (needed for finite element modeling).*
3. *Rank order each of the experimental data sets and calculate the rank probability of failure for each specimen in each data set,*

$$P_{i-rank}^{LC} = \frac{i-0.3}{n_{LC}+0.4}, P_{i-rank}^{HC} = \frac{i-0.3}{n_{HC}+0.4}, \quad (12)$$

where n_{HC} and n_{LC} denote the number of specimens in each data set and i denotes the rank number, respectively (see Bompas-Smith [21]).

4. Perform nonlinear 3-D finite element analyses as described here and in [8,13,20] for:

- both HC and LC test specimen geometries, and
- the plane-strain reference configuration, 1T SSY (T -stress = 0).

The stored, stress-strain results for each element at each analysis load step enable very rapid computation of the Weibull stress value using Eq. (6) for a specified, trial value of m .

5. Assume trial values for m and K_{min} (or assume K_{min} is fixed at 20 MPa \sqrt{m} as in E1921). From 3-D finite element results, compute σ_w vs. J loading curves for the specimens (HC and LC) and for the 1T SSY reference condition. Convert J -values to K_J -values by applying the plane-strain conversion (the calibration process is expressed in terms of K_J to maintain similarity with E1921 terminology). Set the value of $\sigma_{w-min} = \sigma_w(K_J = K_{min})$.
6. Correct the high and low constraint toughness values to the 1T SSY plane-strain condition using Eq. (11). This yields two sets of toughness values termed $K_{Jc}^{HC-1TSSY}$ and $K_{Jc}^{LC-1TSSY}$, or generally as $K_{Jc}^{xC-1TSSY}$.
7. Use Eq. (2) to compute $K_0^{HC-1TSSY}$ for the high constraint data set. Use $K_0^{HC-1TSSY}$ and the trial value of K_{min} to define a continuous, cumulative failure probability function termed here K_{Jc}^{1TSSY} from Eq. (1).
8. For the trial pair m and K_{min} , calculate a scalar error measure to characterize differences between the HC and LC constraint-corrected distributions. The new error measure here includes two parts: (1) the summed differences between the high and low constraint-corrected data sets (Step 6) and the continuous SSY distribution (Step 7); and (2) the summed differences between the K_{Jc} -values for the high and low constraint data sets scaled to SSY (both from Step 6).

$$Error(m, K_{min}) = \sum_{i=1}^{n_{LC}+n_{HC}} \left| K_{Jc(i)}^{xC-1TSSY} - K_{Jc(i)}^{1TSSY} \right| WF_{(i)} + \sum_{i=1}^{\min(n_{LC}, n_{HC})} \left| K_{Jc(i)}^{HC-1TSSY} - K_{Jc(i)}^{LC-1TSSY} \right| WF_{(i)} \quad (13)$$

The multiplier, WF , denotes a weight factor ($\sum WF \equiv 1$), which scales the error contribution for a given value of i based on the confidence in the current failure probability. See the Appendix for additional details including modifications to handle the $n_{HC} \neq n_{LC}$ case.

Other, similar error measures likely would lead to equally satisfactory estimates for the parameters.

9. Repeat steps 5-8 for additional trial pairs of m and K_{min} .

10. The calibrated pair (m, K_{min}) minimizes the error function.

After calibration of m and K_{min} , compute values for σ_u and σ_{w-min} using the finite element results for σ_w vs. J . Remember that σ_u^{1TSSY} corresponds to $K_J = K_0^{1TSSY}$ (Step 7) and σ_{w-min}^{1TSSY} to $K_J = K_{min}$ calculated for the reference configuration. The following equation scales the calibrated σ_u^{1TSSY} to the experimental specimen configuration (xT xC),

$$\sigma_u^{xTxC} = 4/m \sqrt{\sigma_w^{m/4} \left| \sigma_w^{m/4} - \sigma_{w-min}^{m/4} \right| \left| \sigma_w^{m/4} - \sigma_{w-min}^{m/4} \right|^{xTxC}}, \quad (14)$$

where σ_{w-min}^{xTxC} denotes the σ_w value corresponding to $K_J = K_{min}$ for the xT size specimen of interest. Equation (7) may be used to compute σ_{w-min}^{xTxC} if the specimen has not experienced constraint loss at K_{min} , oth-

erwise, use Eq. (8). Using m , σ_u^{xTxC} , and σ_{w-min}^{xTxC} , predictions of the cumulative probability of failure for the xT size specimen at a given temperature follow from Eq. (9).

This page is intentionally blank.

4 Finite Element Modeling

Nonlinear finite element analyses are performed on highly refined meshes using the research code WARP3D [22]. The material response follows a Mises constitutive model with J_2 flow theory-isotropic hardening and includes the effects of large displacements and finite strains. Each finite element model consists of standard three-dimensional, 8-node elements with $2 \times 2 \times 2$ Gauss quadrature and a \bar{B} formulation to prevent volumetric locking. WARP3D includes a domain integral procedure that enables computation of J -integral values point-wise along the front of a crack and the through-thickness average value.

At each temperature, the analyses use piecewise-linear representations of the quasi-static, true stress-true strain curves measured [16,23] for the Euro material — a quenched and tempered pressure vessel steel DIN 22NiMoCr37 similar to ASME Grade A508 Cl.3 (see Fig. 2). The tests and instrumentation enabled logarithmic strain values to reach $\varepsilon = 2.0$; the curves input to WARP3D have no further hardening for $\varepsilon > 2.0$. As commonly observed in ferritic steels, the yield stress decreases slowly with increasing temperature over the DBT region. The complete experimental stress-strain curve at -110°C remained unavailable to us at the time of our analyses; consequently, we adopted the material flow properties at -91°C in analyses for specimens tested at -110°C . Temperature invariant values of $E = 206$ GPa and $\nu = 0.3$ are employed in the analyses. The strong dependency of computed Weibull stress values on the stress-strain fields just ahead of the blunted region along the crack front leads to a direct dependence on details of the stress-strain curves input to the analyses. Preliminary analyses to compute the σ_w - J curves using initial stress-strain curves with measured strains $\varepsilon \leq 0.12$ showed a significant variability depending on the assumptions made for the input curves at larger strain levels (overall load-displacement curves from the analyses show no effect since very small volumes of material at the crack front experience severe straining). The availability of stress strain curves at the higher maximum strain values eliminated this issue.

The plane-strain, SSY stress fields with zero T -stress define a very high constraint, reference condition at the crack front to assess constraint loss in the fracture specimens. To generate these fields, this study employs a standard boundary layer model [24, 25]. At maximum load, the extent of the plastic zone (R_p) remains small compared to the outer boundary radius ($R_p < 0.05R$). The one-quarter symmetric, finite element mesh shown in Fig. 3c contains approximately 2,800 elements with one element layer through the thickness. A plane-strain, Mode I displacement field applied to the outer boundary loads the model,

$$u(R, \theta) = \frac{K_I(1+\nu)}{E} \sqrt{\frac{R}{2\pi}} \cos\left(\frac{\theta}{2}\right) (3 - 4\nu - \cos\theta), \quad (15)$$

$$v(R, \theta) = \frac{K_I(1+\nu)}{E} \sqrt{\frac{R}{2\pi}} \cos\left(\frac{\theta}{2}\right) (3 - 4\nu - \cos\theta), \quad (16)$$

$$w(R, \theta) = 0 \quad (17)$$

The crack-tip region of the SSY mesh has a small initial root radius of $2.5 \mu\text{m}$ to aid convergence of the finite-strain analyses in the early stages of loading. The σ_w - J curves obtained from the SSY analyses enable computation of the C and \bar{C} constants in Eq. (7).

Nonlinear finite deformation analyses are also performed on 3-D models of CVN and C(T) specimen geometries using very refined meshes. Figures 3(a,b) show the one-quarter symmetric finite element meshes defined for these two specimens. The CVNs are 0.4T SE(B)s with a square cross-section, pre-cracked to $a/W = 0.12$ or 0.5 . The proportionally scaled C(T) specimens range in size from 0.5T to 2T, all analyzed with $a/W=0.56$ (the g -function approach described previously enables simple scaling of the 1T size used in the analyses to all other sizes). Focused rings of elements surround the crack-tip region of each specimen. The specimen meshes also contain an initial root radius at the crack front. Under increasing load, extensive element distortion near the notch root prevents convergence of the global Newton iterations. To remedy this problem, several different meshes are employed for each fracture specimen, each mesh has an increasingly larger initial root radius. This process enables generation of solutions over the complete loading history to quite high J -values. The number of elements in the CVN and C(T) models ranges from 16,200 to 28,500 depending on the specimen type and initial root radius, which ranged from 0.25 - $108 \mu\text{m}$ for C(T)s and 0.25 - $36 \mu\text{m}$ for CVNs. The key results (σ_w - J curves) for a mesh are not used until the deformed root radius exceeds $\approx 3\times$ the undeformed radius. Previous work shows that crack-front fields at higher loading then remain unaffected by the initial notch radius [26]. Simple spline fitting of these multi-mesh results yields the final σ_w - J curve for a specimen (at a specific temperature) over the complete load history.

5 Results from Calibration Procedure

5.1 European program

Ten laboratories generated extraordinarily large datasets of fracture toughness values (>800) for a single material during the European Union project entitled “Fracture toughness of steel in the ductile to brittle transition regime.” Heerens *et al.* [16] provide a detailed description of the experimental procedures, material properties, specimen dimensions and locations in the forging. The project participants executed fracture toughness tests using standard, deep notch C(T) specimens with sizes ranging from 0.5T to 4T. The datasets span test temperatures from the lower shelf to the upper shelf with significant coverage of the DBT region. The fracture datasets and experimental stress-strain curves may be downloaded from the GKSS ftp-server at <ftp://ftp.gkss.de/pub/eurodataset>. Subsequent additional work by Heerens *et al.* [17], among others, tested over 400 pre-cracked Charpy specimens machined from the broken halves of 4T C(T)s tested in the Euro-program.

Wallin’s analysis [15] of all the C(T) fracture toughness data generated in the testing program leads to an ASTM E1921 T_0 temperature of -90°C (*i.e.*, the temperature at which the median toughness of a 1T, high-constraint geometry = $100 \text{ MPa}\sqrt{\text{m}}$). Figures 4(a,c) show the rank distributions of cumulative fracture probability, Eq. (12), for the raw experimental fracture toughness values for the 0.5T, 1T, and 2T C(T) specimens at -40°C and at -20°C — temperatures at the upper-end of the DBT region. In contrast, Fig. 4(b) shows the cumulative fracture probabilities for the deep-notch CVN and 0.5T C(T) specimens tested in the lower-transition region at -110°C . Three of the 0.5T C(T)s at -40°C and most of the 0.5T C(T) specimens at -20°C experienced significant, stable ductile tearing prior to cleavage fracture. All other specimens failed by cleavage fracture without measurable ductile tearing. To better characterize the relative amount of deformation in various size specimens across the DBT shown in Fig. 4, markers corresponding to different M -values are provided, where $M = b\sigma_0/J$ with the temperature dependent σ_0 taken from Fig. 2. To place these values in perspective, E1921 requires censoring of values for deep-notch specimens with $M \leq 30$, although some amount of constraint loss does occur at higher M -values, especially in the SE(B) specimens.

Figure 5 shows the distributions of cumulative fracture probability for raw experimental toughness values of datasets used here later to explore the robustness of the calibrated Weibull stress model. These datasets are not used in any present calibrations and include: (1) deep notched ($a/W = 0.5$) CVNs at -91°C ; (2) 0.5T C(T)s at -60°C , and (3) shallow-notched ($a/W = 0.12$) CVNs at -110°C . All deep-notch C(T) specimens in all datasets have a nominal $a/W = 0.56$.

Figure 6 shows the experimental datasets of Fig. 4 scaled to a common, 1T crack-front length using Eq. (4) as described in E1921. This *statistical* adjustment corrects the different datasets at a common temperature to have the same cumulative failure probabilities provided there exists no *deterministic* constraint loss from large-scale yielding effects. In Fig. 6(a) for -40°C , the 2T and 1T datasets merge very closely but the 0.5Ts diverge for specimens with $M \leq 20$. At -20°C in Fig. 6(c), the 0.5T specimens all have $M \leq$

20 and show a markedly different behavior from the 1T and 2T specimens (which also appear to show some constraint differences). Figure 6(b) shows that even at -110°C (20°C below T_0) there appears to exist a constraint difference between deep-notch CVNs and C(T)s with nominally the same crack-front length ($0.4T$ vs. $0.5T$).

5.2 Calibration Strategy

The procedures to calibrate the three-parameter Weibull stress model described in Section 2 rely upon the existence of fracture toughness datasets at a fixed temperature with differing amounts of constraint loss. The present work uses the toughness datasets for the Euro-material measured at -40°C and at -110°C to calibrate the parameters (independently) to investigate the temperature dependence of the Weibull modulus (m). These two test temperatures of $T_0 - 20^{\circ}\text{C}$ and $T_0 + 50^{\circ}\text{C}$ lie at the extreme ends of the DBT for this material and should indicate the temperature effect on m if it exists.

Bernauer *et al.* [27] previously combined a continuum damage model for ductile tearing with the standard, two-parameter Beremin model to calibrate Weibull stress parameters for this same Euro-material. Based on initial quasi-static fracture and tensile tests produced by the program, the calibrated m in [27] varied from 22 to 103 depending on test temperature and specimen geometry. Their results using fracture tests relied on a single set of high-constraint specimens, C(T)s, combined with the maximum likelihood parameter calibration method of Minami *et al.* [11] and thus their results may have been influenced by the non-uniqueness issue [8,12,13]. The calibration process here uses the final, very large datasets combined with a three-parameter Weibull stress model and the constraint-based procedure to overcome the non-uniqueness issues.

5.3 Calibration at -40°C

Here we calibrate the Weibull stress parameters for the Euro-material at -40°C using the $0.5T$ and $1T$ C(T) fracture toughness data (see Fig. 4a). Exceptionally large fracture toughness values ($M \leq 10$) are excluded from the calibration procedure. Excessive deformation occurs along the crack front in the finite element models and predicted strain levels exceed the experimental stress-strain curves input to the analyses. Some specimens with M values ≤ 10 reportedly have ductile tearing not incorporated in the present analyses. The calibration procedure follows the steps outlined in Section 2. Figure 7(a) provides the error function of Eq. (13) over a wide range of trial m and K_{min} pairs (m and K_{min} range from 1 to 30 and from 0 to $80 \text{ MPa}\sqrt{\text{m}}$, respectively). Figure 7(a) illustrates the error as a function of m ; Figure 7(b) shows the corresponding value of K_{min} at each of these m -values that leads to the indicated minimum error. The Eq. (13) error values are normalized by the maximum error value found over the examined range of m and K_{min} . At -40°C , the error function remains relatively constant for values of m ranging from 18 to 22. Similarly, the corresponding K_{min} values remain nearly constant at $40 \text{ MPa}\sqrt{\text{m}}$ for values of m ranging from 18 to 22 (recall that E1921 adopts a temperature invariant $K_{min} = 20 \text{ MPa}\sqrt{\text{m}}$ for all materials to reduce the required number of test specimens to a practical value of 6 minimum).

The Weibull stress parameters $m = 20$ with σ_{w-min} computed at $K_{min} = 40 \text{ MPa}\sqrt{\text{m}}$ appear to best minimize the error function at -40°C . Figure 8(a) illustrates the effects of the now combined *statistical* crack-front length (thickness) adjustment and the *deterministic* constraint correction. Each measured toughness value for the 0.5T and 1T C(T) specimens is corrected to an equivalent 1T SSY value using Eq. (11), where the g -function corresponds to the calibrated $m = 20$ (for the C(T) geometry and stress-strain curve at -40°C) and K_{min} equals the calibrated value of $40 \text{ MPa}\sqrt{\text{m}}$. The rank probabilities (P_f) follow from Eq. (12). The continuous curve on the figure represents Eq. (9) based on these values: $m = 20$, σ_{w-min} computed at $K_{min} = 40 \text{ MPa}\sqrt{\text{m}}$ in the 1T-SSY boundary layer model, and $\sigma_u = \sigma_w$ at $K_J = K_0^{1TSSY}$ for the 1T-C(T) specimen (see Step 7 in the calibration process). Table 1 lists the computed values of σ_u and σ_{w-min} for each specimen and \bar{C} . The P_f value for each σ_w value is plotted in terms of the corresponding K_J^{1TSSY} value computed with Eq. (7) given \bar{C} at -40°C (and a unit value for V_0).

These constraint corrected values in Fig. 8(a) should be compared to those in Fig. 6(a), which reflect only the (statistical) crack-front length adjustment. Since this m and K_{min} pair minimizes the error function based on constraint differences, the constraint corrected toughness values collapse to essentially the same distribution in Fig. 8(a) as expected. For reference, Fig. 8(b) shows the constraint corrected values for the same datasets but using a very different pair of Weibull stress parameters of $m = 4$ and $K_{min} = 20 \text{ MPa}\sqrt{\text{m}}$. Here the corrected datasets do not collapse to same distributions indicating an incorrect pair of values (m , K_{min}).

Figures 9(a,c) show the cumulative probability of fracture predictions for the 0.5T, 1T and 2T C(T) specimens using the calibrated parameters. The raw experimental toughness values (no adjustments, no corrections) are plotted at the corresponding rank probability values in each case. The continuous curve for each dataset derives from Eq. (9) based on these values: $m = 20$, σ_{w-min} computed at $K_{min} = 40 \text{ MPa}\sqrt{\text{m}}$ in the 1T-SSY boundary layer model, and $\sigma_u = \sigma_w$ at $K_J = K_0^{1TSSY}$ for the 1T-C(T) specimen and adjusted via Eq. (14) to the actual specimen size (see Step 7 in the calibration process). Table 1 lists the computed values of σ_u and σ_{w-min} for each specimen. The P_f value for each σ_w value is plotted in terms of the corresponding K_J^{xT} value where σ_w values are computed with Eq. (8) given \bar{C} at -40°C (and a unit value for V_0). The g -function for each of these proportionally-sized C(T) specimens is identical. This process, based on the calibrated Weibull stress parameters, leads to consistent predictions for the 0.5T and 1T C(T) specimens as indicated in Fig. 9a, *i.e.* the data used to calibrate the parameters. The predicted distribution for the 2T C(T) dataset (not used in the calibration) shows excellent agreement as well.

5.4 Calibration at -110°C

We repeat the above calibration procedure using large datasets of 0.5T C(T) and deep notch, pre-cracked CVN specimens at -110°C . At this temperature, 20°C below $T_0 = -90^\circ\text{C}$, even the small C(T) specimens exhibit very nearly SSY behavior at fracture. Consequently, the absence of constraint loss between, for example, 1T and 0.5 C(T) specimens precludes calibration of the Weibull stress parameters. Figure 6(b) shows the 0.5T C(T) and CVN datasets adjusted to (statistically) equivalent 1T thickness using the E1921 procedure. The resulting distributions indicate sufficient constraint loss exists in the pre-cracked CVN specimens (0.4T SE(B)s with $B \times B$ cross-section) to calibrate the parameters.

Figure 7(c) provides values of the error function defined in Eq. (13) over a wide range of trial m and K_{min} pairs (m and K_{min} range from 1 to 30 and from 0 to 80 MPa \sqrt{m} , respectively). Figure 7(c) illustrates the error as a function of m ; Figure 7(d) shows the corresponding value of K_{min} at each of these m -values that leads to the minimum error. Here the Eq. (13) error values are again normalized by the maximum error value found over the examined range of m and K_{min} . The reduced level of constraint loss for these two specimen geometries (compared to the specimens used at -40°C) leads to less “sensitivity” in the calibration process. This effect appears as the larger “flat” region of the error curve in Fig. 7(c). As the constraint difference between the two datasets used in the calibration gradually vanishes, all values of m fit the datasets indicating the loss of uniqueness discussed in [8,12,13].

Figures 7(c,d) indicate that $m = 18$ and $K_{min} = 30$ MPa \sqrt{m} minimize the error at this temperature. Figure 8(d) illustrates the effects of the now combined *statistical* crack-front length (thickness) adjustment and the *deterministic* constraint correction. Each measured toughness value for the 0.5T C(T) and the CVN specimen is corrected to an equivalent 1T-SSY value using Eq. (11) and K_{min} equals the calibrated value of 30 MPa \sqrt{m} . Since m and K_{min} minimize the error function, the constraint corrected toughness values collapse to nearly identical distributions. For reference, Fig. 8(d) shows the constraint corrected values for the same datasets but using a very different pair of Weibull stress parameters of $m = 4$ and $K_{min} = 20$ MPa \sqrt{m} . Here the corrected datasets do not collapse to same distributions indicating an incorrect pair of values (m, K_{min}).

Figure 9(b) shows the cumulative probability of fracture predictions for the 0.5T C(T) and CVN specimens using the calibrated parameters. The raw experimental toughness values (no adjustments, corrections) are plotted at the corresponding rank probability values in each case. The continuous curve for each dataset derives again from Eq. (9) based on these values: $m = 18$, σ_{w-min} computed at $K_{min} = 30$ MPa \sqrt{m} in the 1T-SSY boundary layer model, and $\sigma_u = \sigma_w$ at $K_J = K_0^{1TSSY}$ for the 0.5T-C(T) specimens and adjusted via Eq. (14) to the actual specimen size (see Step 7 in the calibration process). Table 1 lists the computed values of σ_u and σ_{w-min} for each specimen and \bar{C} . The P_f value for each σ_w value is plotted in terms of the corresponding K_J^{xT} value where σ_w values are computed with Eq. (8) given \bar{C} at -110°C (and a unit value for V_0). The predicted distributions for these two datasets, both used in the calibration, show excellent agreement as expected.

5.5 Consequences of Temperature Invariant m -Value

Based on the independent calibrations using very large datasets at extremes of the DBT (-40°C , -110°C), the Weibull modulus, m , appears to remain essentially invariant of temperature with a value of 18 to 20 for this key ferritic steel used to fabricate many commercial reactor pressure vessels. Further, the best-fit K_{min} value appears to increase slowly with temperature while σ_u increases more sharply with temperature over the DBT region. These results are consistent with recent studies by Petti and Dodds [14]. In a related effort, Gao and Dodds [28] show, through similar calibrations, an invariance of m to loading rate at a fixed temperature in the DBT for a strongly rate-sensitive ferritic steel (A515-70). Not surprisingly, they find that σ_u exhibits a dependence on loading rate (decreases with increased K -rate) but insufficient experimental data precludes a study of the K_{min} rate dependence in their work.

The temperature invariance of m opens the real potential for practical applications of this methodology to quantify constraint effects on cleavage toughness over the DBT region. Experimental datasets with sufficient constraint difference are then required at only one temperature to calibrate m . Petti and Dodds [14] outline a new procedure to predict the cumulative probabilities of fracture at any temperature over the DBT region for specimen geometries that experience constraint loss given a calibrated value for m and an estimated or assumed variation for K_{min} with temperature (could be simply a constant value of, for example, 20 MPa \sqrt{m}). In the Petti and Dodds approach, the toughness-temperature relationship defined by the E1921 Master Curve for K_{Jc} enables computation of the σ_u temperature dependence — the process forces the Weibull stress model with a calibrated, temperature invariant m value to predict the E1921 Master Curve K_{Jc} -temperature dependence.

In the next section, we employ the present calibrated Weibull stress parameters for the Euro-material and the Petti and Dodds procedure to predict the measured fracture distributions at various temperatures over the DBT region not used in the present calibrations. This exercise thus very closely represents a likely application scenario in practical defect assessments.

This page is intentionally blank.

6 Predictions Over DBT by Coupling with the Master Curve

The previous section used extensive fracture data sets for the Euro-material to demonstrate that the Weibull modulus (m) remains essentially constant over the DBT range (≈ 20 at -40 °C and ≈ 18 at -110 °C). The experimental toughness values at these two temperatures, coupled with known m -values, also enabled determination of temperature specific σ_u and K_{min} values (and thus σ_{w-min}). In practical defect assessments, such temperature specific calibrations become impractical. Most likely, sets of low and high constraint fracture toughness values for the calibration process will be available at only one temperature.

With the knowledge that m remains essentially constant over the DBT range for this important pressure vessel steel, this section describes an application of the Petti and Dodds procedure [14] to predict cumulative fracture probabilities for specimens that experience constraint loss. The recommended procedure uses the calibrated value of m for the material obtained from fracture toughness tests conducted above T_0 (but below the onset of ductile tearing) to maximize the constraint loss in the datasets and thereby increase the calibration sensitivity. Recall that when the temperature falls well below T_0 the behavior of all fracture specimens approaches SSY (including small-sized specimens and specimens with shallow-cracks). Once SSY conditions are reached, a unique calibration of the Weibull stress parameters is no longer possible (see extended discussions in [8,15,19]). The present calibration process thus relies on the large differences in fracture toughness between high and low constraint specimens that develop rapidly at temperatures above T_0 . Predictions from the calibrated model at lower temperatures, approaching and below T_0 , are then expected to maintain accuracy as all datasets gradually merge to the SSY condition on the lower-shelf at which m becomes a non-unique parameter

The large datasets of fracture toughness values with some constraint loss available for the Euro-material over the DBT region between -20 °C and -110 °C provide a unique opportunity to assess the practicality and effectiveness of the proposed procedure. Let us assume then for this exercise that high and low fracture toughness datasets are available only at -40 °C. The high toughness dataset, the 1T C(T) specimens, combined with conventional application of the ASTM E1921 procedures leads to an estimate of the reference temperature $T_0 \approx -90$ °C. Using the high constraint 1T C(T) specimens and the 0.5T C(T) specimens (which experience some constraint loss), the calibrated Weibull modulus again becomes $m = 20$, as developed in Section 5.3. In practice, the number of available test specimens for the calibration (often 6–10) would be far less than the number of specimens here for the Euro-material at -40 °C. The reduced number of specimens in practice would thus preclude the simultaneous calibration of K_{min} , which is set now at the temperature invariant value of $20\text{MPa}\sqrt{\text{m}}$, as required in E1921, rather than the calibrated value of $40\text{MPa}\sqrt{\text{m}}$.

With m and K_{min} now known over the full DBT range, the only remaining parameter required to estimate fracture probabilities at temperatures other than -40 °C becomes the Weibull scale parameter, σ_u , which varies with temperature. The procedure outlined by Petti and Dodds [14] predicts σ_u as a function of temperature using the calibrated m -value and the known value for T_0 . Given T_0 , the procedure adopts the

E1921 Master Curve to estimate the scale parameter K_0^{1T} (assumed to represent plane-strain 1T SSY conditions) as a function of temperature. Finite element analyses of the plane-strain SSY boundary layer model over a range of temperatures yield the Weibull stress vs. K_J curves and thus the constant \bar{C} for use in Eq. (7). The finite element analyses of the SSY model and of the application geometries do require the measured, uniaxial stress-strain curves at the specific application temperatures. The analyses and K_0^{1T} estimates from the Master Curve enable computation of the needed σ_u values as a function of temperature. With σ_u known, the cumulative fracture probabilities for the application geometry may be computed using the procedures described in Section 5.

Here, we employ this procedure to estimate the cumulative fracture probabilities of the Euro-material for these configurations that have some level of constraint loss: (a) shallow notch CVN specimens at -110°C , (b) deep-notch CVN specimens at -91°C , (c) 0.5T C(T) specimens at -60°C , and (d) 2T, 1T and 0.5T C(T)s at -20°C . Large datasets of measured fracture toughness values are available at each of these conditions for the Euro-material to assess the reliability of this approach — none of these datasets have been used in any calibration processes described in this work.

The following steps describe the procedure in additional detail:

1. Calibrate the Weibull stress parameter m as described in Section 3 using datasets of fracture toughness obtained at a temperature above T_0 but below the onset of significant ductile tearing (recommended). The calibrated m -value then remains invariant of temperature. Most often, K_{min} will be set to the temperature invariant, E1921 value of $20 \text{ MPa}\sqrt{\text{m}}$. Here, we use the calibrated value of $m = 20$ at -40°C .
2. Use the high constraint experimental data from the calibration and calculate the E1921 reference temperature T_0 ,

$$T_0 = T - \frac{1}{0.019} \ln \left[\frac{K_{Jc(\text{med})}^{1T} - 30}{70} \right] \text{ MPa}\sqrt{\text{m}}, \text{ } ^\circ\text{C}, \quad (18)$$

where T denotes the test temperature and

$$K_{Jc(\text{med})}^{1T} = 0.9124(K_0^{1T} - K_{min}) + K_{min} \text{ MPa}\sqrt{\text{m}}, \quad (19)$$

with

$$K_0^{1T} = \left[\sum_{i=1}^N \frac{(K_{Jc(i)}^{1T} - K_{min})^4}{(N - 0.3068)} \right]^{1/4} + K_{min} \text{ MPa}\sqrt{\text{m}}, \quad (20)$$

where N denotes the number of specimens in the dataset.

3. Using the Master Curve and T_0 , calculate K_0^{1T} for the DBT temperature(s), T , at which predictions of fracture probabilities for specimens with constraint loss are desired,

$$K_0^{1T} = 31 + 77 \exp[0.019(T - T_0)] \text{ MPa}\sqrt{\text{m}}, \text{ } ^\circ\text{C}. \quad (21)$$

4. Using stress-strain curves at the application temperatures, perform finite element analyses to compute Weibull stress values (with calibrated m) for: (a) the 1T plane-strain SSY reference condition, (b) all specimens (sizes and geometries) of interest.

5. Find the value of σ_u^{1T} corresponding to $K_I = K_0^{1T}$ and σ_{w-min} corresponding to $K_I = K_{min}$ for the desired temperature using results from the 1T plane-strain SSY analysis.
6. Calculate the denominator of Eq. (9), $\sigma_{u(1TSSY)}^{m/4} - \sigma_{w-min(1TSSY)}^{m/4}$, for the application temperature. This value remains constant with changes in constraint (e.g. specimen size and type). Though not needed to make the predictions, the value of σ_u for the specimen of interest follows from Eq. (14).
7. Using results from the finite element analyses of the specimens, calculate σ_{w-min}^{xT} .
8. Use Eq. (9) with the constant denominator calculated in Step 6, the value of σ_{w-min}^{xT} for the specimen of interest calculated in Step 7, and the xT specimen's Weibull stress distribution as a function of K_I from Step 4 to predict the distribution of cumulative fracture probability P_f vs. K_I .

From Step 3 above and with $T_0 = -90^\circ\text{C}$, K_0^{1T} (assumed here to be plane-strain SSY) equals 106.5 MPa $\sqrt{\text{m}}$, 167.2 MPa $\sqrt{\text{m}}$, and 322 MPa $\sqrt{\text{m}}$ at -91°C , -60°C , and -20°C , respectively. Application of the remaining steps of the procedure leads to predictions of the cumulative fracture probabilities for the lower-constraint geometries across the DBT range. Petti and Dodds [14] discuss the potential consequences of assuming that the Master Curve actually represents 1T, plane-strain SSY conditions — at temperatures in upper transition this strong connection diminishes and also contributes to errors in predictions of fracture probabilities at temperatures higher than the one used to calibrate m . A quantitative recommendation on the upper limit of testing temperature above T_0 is not possible with this technology at the present time. The current model (faithfully) reproduces built-in inaccuracies of the Master Curve shape at temperatures approaching upper transition.

Figure 10(a) compares the predictions to the raw experimental data at -91°C for the deep notch CVNs. The Weibull stress-based prediction (curve) very closely matches the rank probability values for the measured experimental toughness values. Figure 10(b) illustrates equally good agreement for the 0.5T C(T) specimens at -60°C . Figure 10(c) illustrates the predictions at -20°C for the 2T, 1T and 0.5T C(T) specimens. The circles indicate those 0.5T C(T) specimens, which experienced ductile tearing prior to fracture. In the finite element analyses, excessive deformation along the crack front in these 1T and 0.5T C(T) specimens at -20°C for very high toughness levels eventually limits the accuracy of the predictions. Nevertheless, the method produces reasonably good predictions of the cumulative probability of failure for these specimens at 70°C above T_0 and at 20°C above the temperature used for calibration of m . Finally, Figure 10(d) shows the predictions for the newly available shallow-notch ($a/W = 0.12$) CVN specimens tested at -110°C . The solid line illustrates the prediction using the E1921 value of 20 MPa $\sqrt{\text{m}}$ for K_{min} . For reference, the dashed line shows the improved prediction for the temperature specific, calibrated value of $K_{min} = 30$ MPa $\sqrt{\text{m}}$ described in Section 4.4.

The good agreement of predictions with measured experimental toughness values shown in each case in Fig. 10 provides an encouraging demonstration for application of the Weibull stress method, at least for this key ferritic steel used in many nuclear pressure vessels. The demonstrated temperature invariance of the Weibull modulus, m , coupled with a fixed K_{min} and the E1921 Master Curve to support temperature dependent σ_u represents a reasonably practical engineering methodology.

This page is intentionally blank.

7 Summary and Conclusions

This study utilizes the very large datasets of more than 800 specimens from a recently completed European Union research project entitled “Fracture toughness of steel in the ductile to brittle transition regime” to investigate the temperature dependence of the Weibull stress modulus, m , over the ductile-to-brittle transition range. The material is a widely used, nuclear pressure vessel steel DIN 22NiMoCr37 (similar to the American A508 Cl.3 steel). The Weibull stress micromechanical model for cleavage fracture adopted in this study has three-parameters in the expression for the cumulative fracture probability that require calibration: the modulus m , the scale factor σ_u and a threshold value, σ_{w-min} , of the Weibull stress below which cleavage fracture does not occur. Once these parameters become known for a material at a specified temperature over the DBT range, 3-D finite element analyses of fracture specimens may be used to predict cumulative probabilities of cleavage fracture under various levels of constraint loss that develop from large-scale plasticity.

The work presented here supports the following conclusions:

- Sufficient constraint difference exists in the available experimental datasets to calibrate the Weibull modulus, m , at the extreme range of temperatures of the DBT for this material. The ASTM E1921 reference temperature $T_0 = -90^\circ\text{C}$. Independent calibrations of m are described in this study at $T = -40^\circ\text{C}$ and -110°C .
- The calibrated m -values are $m = 20$ at $T = -40^\circ\text{C}$ and $m = 18$ at $T = -110^\circ\text{C}$, with greater sensitivity of the calibration process demonstrated at the higher temperature. The calibration process selects the value for m that collapses datasets with constraint differences to have the same distributions of cumulative fracture probability in a 1T, plane-strain SSY reference condition. Based on these results derived from exceptionally large datasets, we conclude that m for this key ferritic steel remains invariant of temperature over the DBT range.
- The very large datasets support simultaneous estimates for the best-fit value of the threshold toughness, K_{min} , as used in the E1921 three-parameter Weibull expression for the cumulative fracture probability. The best-fit values are $K_{min} = 30 \text{ MPa}\sqrt{\text{m}}$ at $T = -110^\circ\text{C}$ and $K_{min} = 40 \text{ MPa}\sqrt{\text{m}}$ at $T = -40^\circ\text{C}$. ASTM E1921 recommends use of a temperature invariant value of $K_{min} = 20 \text{ MPa}\sqrt{\text{m}}$ unless quite large datasets are available for the calibration. Not surprisingly, K_{min} does increase somewhat with temperature for this material.
- With calibrated values of the Weibull modulus, m , at $T = -110^\circ\text{C}$, -40°C , corresponding temperature dependent σ_u and σ_{w-min} values derive from nonlinear finite element analyses of the 1T, plane-strain SSY reference condition and of various fracture specimens. The calibrated model predicts correctly the fracture toughness probability distributions for the combined *deterministic* effects of constraint loss and statistical effects of crack-front length at the two calibration temperatures.

- The temperature invariance of the Weibull modulus, m , for this pressure vessel steel makes possible more practical, “engineering” applications of the present Weibull stress model in defect assessments. The modulus, m , is calibrated at a single temperature from test data (recommended to be above T_0 but below the temperature at which significant ductile tearing develops prior to cleavage fracture). Here, we use $m = 20$ from the calibration at $T = -40^\circ\text{C}$. With m and T_0 known, along with stress-strain curves at temperatures of interest over the DBT region, this work demonstrates use of the E1921 Master Curve to compute the temperature dependence of σ_u for the Euro-material. As would be most likely done in practice, K_{min} is fixed over the DBT range at the E1921 recommended value of $20 \text{ MPa}\sqrt{\text{m}}$.
- Applications of this “engineering” approach to additional, large datasets for the Euro-material over the DBT range that show some constraint loss lead to excellent predictions of the measured, cumulative fracture probabilities. These comparisons use no datasets involved in any calibrations of the Weibull stress parameters.

References

1. Test method for the determination of reference temperature T_0 for ferritic steels in the transition range (ASTM E1921), American Society for Testing and Materials, Philadelphia, 2002.
2. Wallin K. Fracture toughness transition curve shape for ferritic steels. Fracture of engineering materials and structures. Elsevier 1991. p. 83-88.
3. Wallin K. Irradiation damage effects on the fracture toughness transition curve shape for reactor pressure vessel steels. Int J Press Ves Piping 1993;55:61-79.
4. Wallin K, Saario T, Torronen K. Statistical model for carbide induced brittle fracture in steel. Metal Science 1984;18:13-16.
5. Wallin K. The scatter in K_{Ic}-results. Engng Fract Mech 1984;19:1085-1093.
6. Beremin FM. A local criterion for cleavage fracture of a nuclear pressure vessel steel. Metallur Trans 1983;14A:2277-2287.
7. Bakker A, Koers RWJ. Prediction of cleavage fracture events in the brittle-ductile transition region of a ferritic steel. In: Blauel, Schwalbe, editors. Defect Assessment in Components – Fundamentals and Applications, ESIS/EG9, Mechanical Engineering Publications, London, 1991. p. 613-632.
8. Gao X, Ruggieri C, Dodds RH. Calibration of Weibull stress parameters using fracture toughness data. Int J Fract 1998;92:175-200.
9. Kroon M, Faleskog J. A probabilistic model for cleavage fracture with a length scale-influence of material parameters and constraint. Int J Fract 2002;118:99-118.
10. Kroon M, Faleskog J. A probabilistic model for cleavage fracture-parameter estimation and predictions of stationary crack experiments. Engng Fract Mech 2004;71:57-79.
11. Minami F, Bruckner-Foit A, Munz D, Trollidenier B. Estimation procedure for the Weibull parameters used in the local approach. Int J Fract 1992;54:197-210.
12. Ruggieri C, Dodds RH. Numerical evaluation of probabilistic fracture parameters with WSTRESS. Engr Comp 1998;15:49:73.
13. Ruggieri C, Gao X, Dodds RH. Transferability of elastic-plastic fracture toughness using the Weibull stress approach: significance of parameter calibration. Engng Fract Mech 2000;67:101-117.
14. Petti JP, Dodds RH. Calibration of the Weibull stress scale parameter, σ_u , using the Master Curve. Engng Fract Mech 2005;72:91-120.
15. Wallin K. Master curve analysis of the “Euro” fracture toughness dataset. Engng Fract Mech 2002;69:451-481.

16. Heerens J, Hellmann D. Development of the Euro fracture toughness dataset. *Engng Fract Mech* 2002;69:421-449.
17. Heerens J, Hellmann D. Fracture Toughness Determination in the Ductile-to-Brittle Transition Regime - Pre-Cracked Charpy Specimens Compared with Standard Compact Specimens. *ESIS-30, Mechanical Engineering Publications*, 2002. p. 297-305.
18. Petti JP, Dodds RH. Coupling of the Weibull stress model and macroscale models to predict cleavage fracture. *Engng Fract Mech* 2004;71:2079:2103.
19. Gao X, Dodds RH. Constraint effects on the ductile-to-brittle transition temperature of ferritic steels: a Weibull stress model. *Int J Fract* 2000;102:43-69.
20. Gao X, Dodds RH, Tregoning RL, Joyce JA, Link RE. A Weibull stress model to predict cleavage fracture in plates containing surface cracks. *Fatigue Fract Engng Mater Struct* 1999;22: 481-493.
21. Bompas-Smith JH. *Mechanical survival: the use of reliability data*. New York, McGraw-Hill, 1973.
22. Koppenhoefer K, Gullerud A, Roy A, Roychowdhury S, Dodds RH. WARP3D: dynamic non-linear analysis of solids using a preconditioned conjugate gradient software architecture. *Structural Research Series (SRS) 596, UILU-ENG-94-2017*, University of Illinois at Urbana-Champaign, 2005.
23. Bernauer G, Brocks W. Micro-mechanical modeling of ductile damage and tearing - results of a European round robin. *Fatigue Fract Engng Mater Struct* 2002;25;363-383.
24. Moran B, Shih CF. A general treatment of crack tip contour integrals. *Int J Fract* 1987;35:295-310.
25. Larsson SG, Carlsson AJ. Influence of non-singular stress terms and specimen geometry on small scale yielding at crack-tips in elastic-plastic materials. *J Mech Phys Solids* 1973;21:447-73.
26. Dodds R, Shih C, Anderson T. Continuum and micro-mechanics treatment of constraint in fracture. *Int J Fract* 1993;64:101-133.
27. Bernauer G, Brocks W, Schmitt W. Modifications of the Beremin model for cleavage fracture in the transition region of a ferritic steel. *Engng Fract Mech* 1999;64:305-325.
28. Gao X, Dodds RH. Loading rate effects on parameters of the Weibull stress model for ferritic steels. *Engng Fract Mech* 2005;72;2416-2425.
29. Wallin K. Optimized estimation of the Weibull distribution parameters. *Research Report 604, Technical Research Center of Finland, Espoo, Finland*, 1989.
30. Rossoll A. Fracture toughness determination of a low alloy steel by instrumented Charpy impact tests. *Ph.D. Thesis, Ecole Centrale des Arts et Manufactures, Chatenay-Malabry, France*, 1998.

Appendix: Calibration Error Measure

The present calibration method employs an updated error measure (function) to characterize differences between the low-constraint (LC) and high-constraint (HC) data sets once they are constraint corrected to the 1T SSY condition for a trial value of m and K_{min} . This procedure also accommodates a variable or fixed value for K_{min} . The error function combines *equally* three contributions as

$$Error(m, K_{min}) = \sum_{i=1}^{n_{LC}} \left| K_{Jc(i)}^{LC-1TSSY} - K_{Jc(i)}^{1TSSY} \right| WF_{(i)} + \sum_{j=1}^{n_{HC}} \left| K_{Jc(j)}^{HC-1TSSY} - K_{Jc(j)}^{1TSSY} \right| WF_{(j)} + \sum_{k=1}^{\min(n_{LC}, n_{HC})} \left| K_{Jc(k)}^{HC-1TSSY} - K_{Jc(k)}^{LC-1TSSY} \right| WF_{(k)} \quad (A1)$$

where n_{LC} and n_{HC} denote the number of test specimens in the LC and HC data sets, respectively. As noted in Section 3, there are likely other, equally effective scalar measures of the calibration error. The one above is physically motivated to reflect data sets with a larger number of values and to (possibly) improve upon the earlier measure of Gao and Dodds [20] based on agreement of only K_0 values for the data sets. Equation (A1) contains three independent parts calculated separately for a trial pair (m, K_{min}) . The first and second parts follow as,

$$\sum_{i=1}^{n_{LC}} \left| K_{Jc(i)}^{LC-1TSSY} - K_{Jc(i)}^{1TSSY} \right| WF_{(i)} + \sum_{j=1}^{n_{HC}} \left| K_{Jc(j)}^{HC-1TSSY} - K_{Jc(j)}^{1TSSY} \right| WF_{(j)} \quad (A2)$$

and compute the difference between the high and low constraint experimental data sets constraint corrected to the reference configuration, $K_{Jc(i)}^{HC-1TSSY}$, and the SSY distribution of $K_{Jc(i)}^{1TSSY}$, see Fig. A1a. The reference (continuous) cumulative failure probability, $K_{Jc(i)}^{1TSSY}$, follows from Eq. (1) using K_0^{1TSSY} taken equal to $K_0^{HC-1TSSY}$. For each specimen toughness value i , the difference between $K_{Jc(i)}^{HC-1TSSY}$ and $K_{Jc(i)}^{1TSSY}$ is thus computed at the same failure probability.

The second part of the error function,

$$\sum_{k=1}^{\min(n_{LC}, n_{HC})} \left| K_{Jc(k)}^{HC-1TSSY} - K_{Jc(k)}^{LC-1TSSY} \right| WF_{(k)} \quad (A3)$$

captures the difference between the high constraint data set values, $K_{Jc(i)}^{HC-1TSSY}$, and the low constraint data set values, $K_{Jc(i)}^{LC-1TSSY}$, where both distributions are constraint corrected to the 1T SSY reference condition. Following the first two parts of the error function, the difference is calculated at equal failure probabilities. For LC and HC data sets with differing numbers of tested specimens (*e.g.* unequal failure probabilities for a given toughness value), we use linear interpolation to estimate the required toughness.

The weight function, WF , reduces the relative contribution of the experimental data with the largest uncertainty in P_f (the tail and top of the distribution),

$$WF_{(i)} = 1 - \frac{CL_{K_{Jc}}(z_i)}{\sum_{i=1}^N CL_{K_{Jc}}(z_i)}, \text{ where } WF^{max} \Rightarrow 1 \quad (A4)$$

and $CL_{K_{Jc}}$ denotes the confidence limit for each sample and N denotes the total number of specimens in the data set. Another possible weight function has a simpler form

$$WF_{(i)} = 1 - \frac{CL_{K_{Jc}}(z_i)}{CL_{K_{Jc}}^{max}(z_i)}, \text{ where } WF^{max} \Rightarrow 1 \quad (\text{A5})$$

and $CL_{K_{Jc}}^{max}$ is the confidence limit for the data value with the most uncertainty. This second weight function should be applied if it is desired to completely reduce the contribution of the data with the most uncertainty.

The weight function is calculated separately for each data set

$$CL_{K_{Jc}}(z_i) = z_i^{95\%} + z_i^{5\%}. \quad (\text{A6})$$

The 5% ($z_i^{5\%}$) and 95% ($z_i^{95\%}$) confidence limits follow from nonlinear equation

$$e_p(z_i) \pm A(z_i)\sqrt{P_e(z_i) - P_e(z_i)^2} = 0, \quad (\text{A7})$$

where

$$e_p(z_i) = \sqrt{\frac{N}{2}}(P_{rank} - z_i), \quad (\text{A8})$$

$$P_e = P_{rank} - \sqrt{\frac{1}{2}}(P_{rank} - z_i), \quad (\text{A9})$$

$$A(z_i) = \min\{1.162 - 0.342/N; 0.82 + P_e \ln(N)\} \text{ for } P_e \leq 0.5, \quad (\text{A10})$$

and

$$A(z_i) = \min\{1.162 - 0.342/N; 0.82 + (1 - P_e) \ln(N)\} \text{ for } P_e > 0.5. \quad (\text{A11})$$

The positive sign in Eq. (A7) corresponds to the 5% limit and the negative sign to the 95% limit. See Wallin [29] and Gao *et al.* [20] for additional details regarding confidence limits.

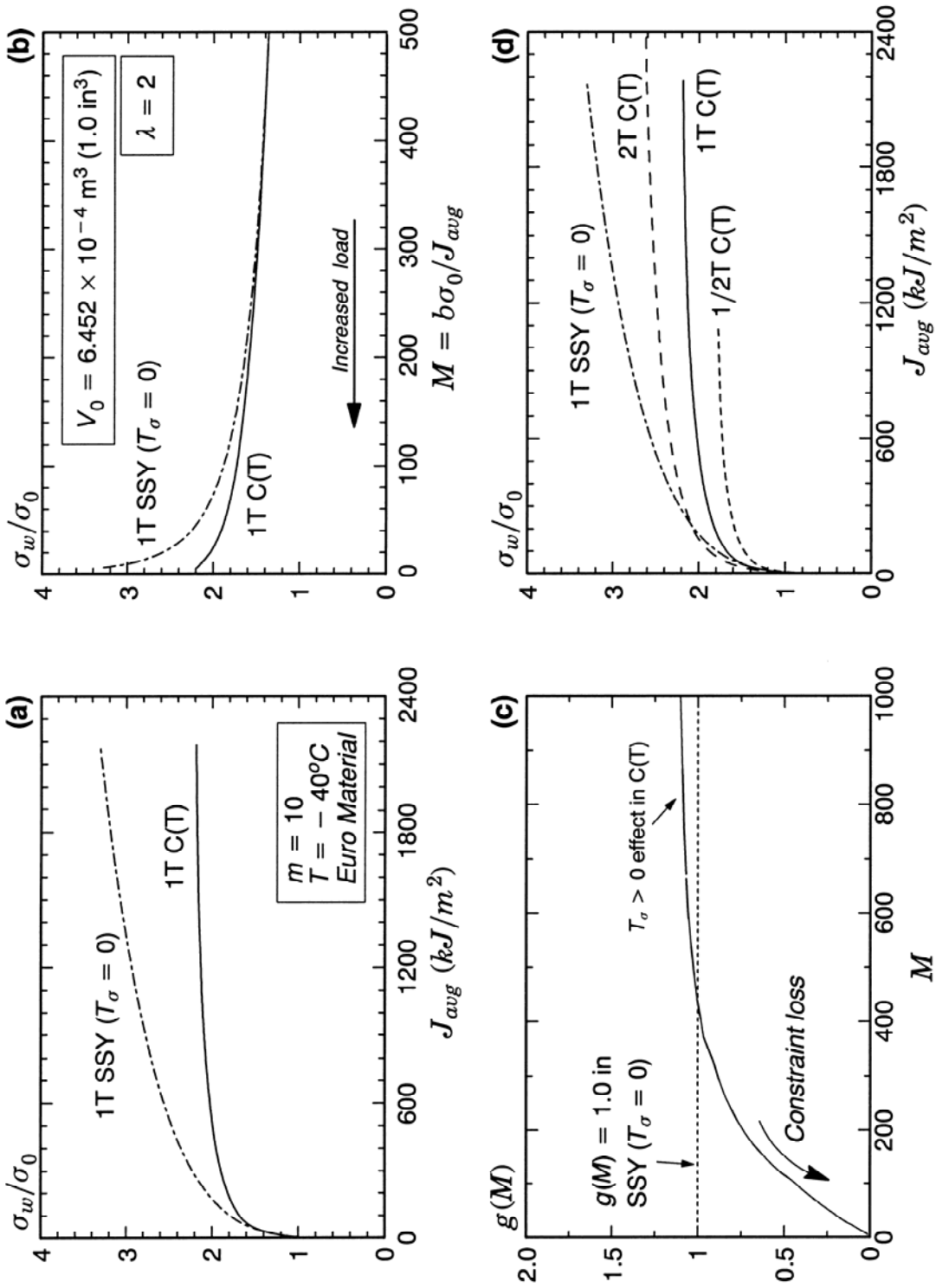


Figure 1. Weibull stress values and constraint correction g -functions computed using stress-strain properties for the Euro material at $-40^\circ C$. Weibull stress modulus taken as $m = 10$ for these illustrative results.

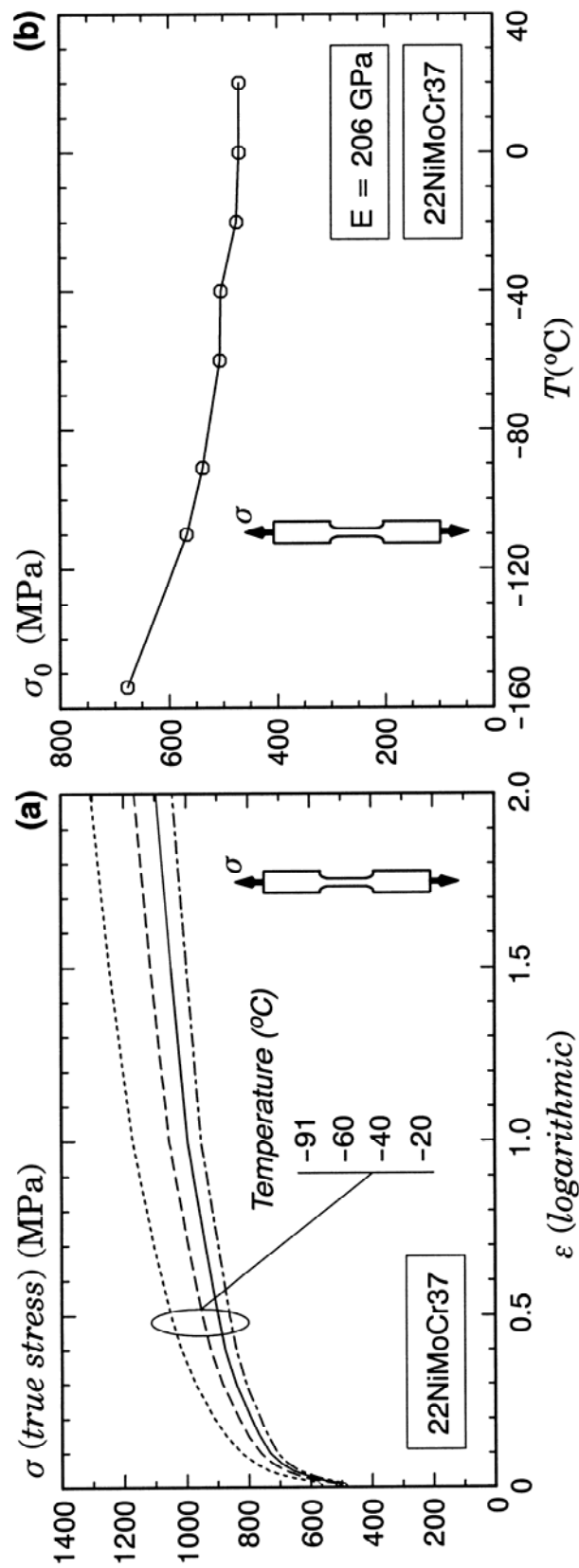
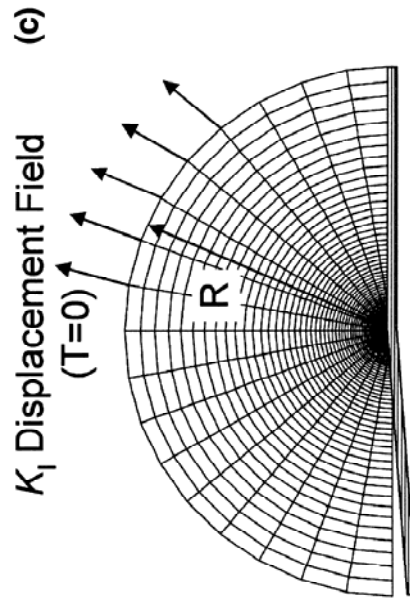
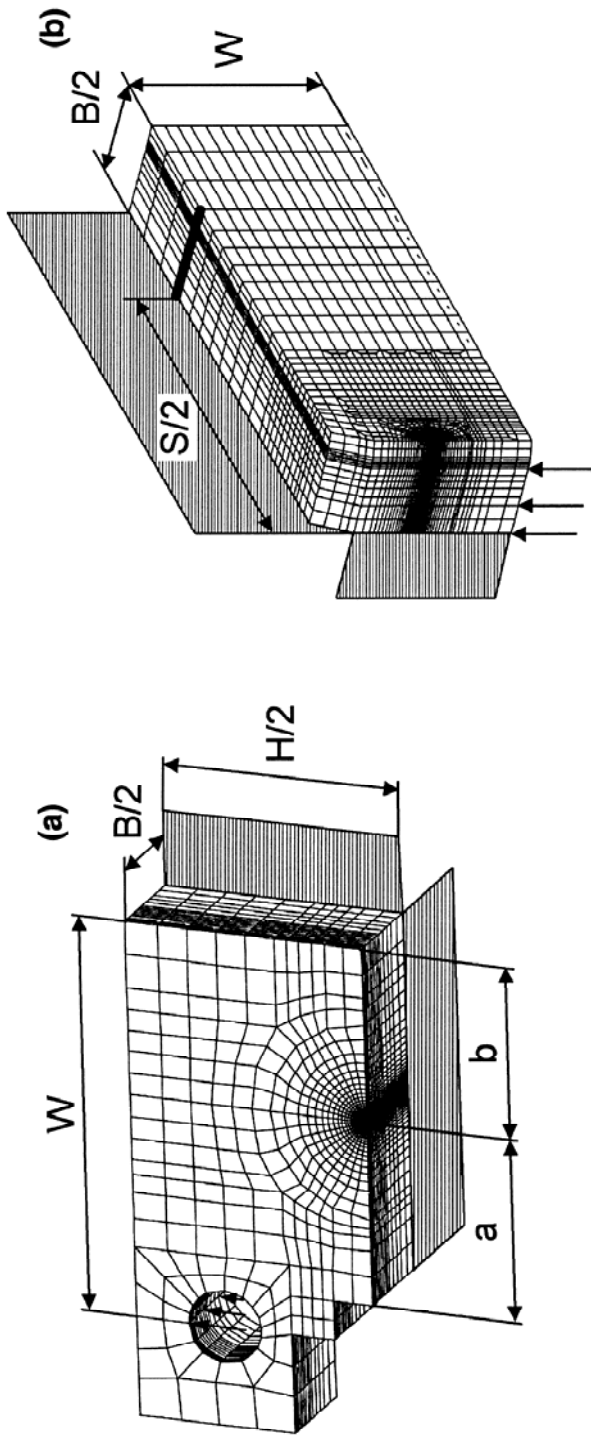


Figure 2. Quasi-static, uniaxial stress-strain curves for Euro-program material (22NiMoCr37 pressure vessel steel). (a) true stress-logarithmic strain curves over a range of temperatures in the DBT region; and (b) yield stresses measured over the DBT region.



Model Size

Model	Number of Elements
C(T)	16,208-27,408
CVN	23,450-28,490
SSY	2771

The number of elements for each specimen varies with the root radii used in various models to obtain the solutions from small to very large deformations.

Figure 3. One-quarter symmetric finite element models for (a) C(T) specimen with $a/W = 0.56$, (b) pre-cracked, 0.4T Charpy V-Notch specimen with $a/W = 0.56$, and (c) small-scale yielding (SSY). All models have finite root radius along crack front.

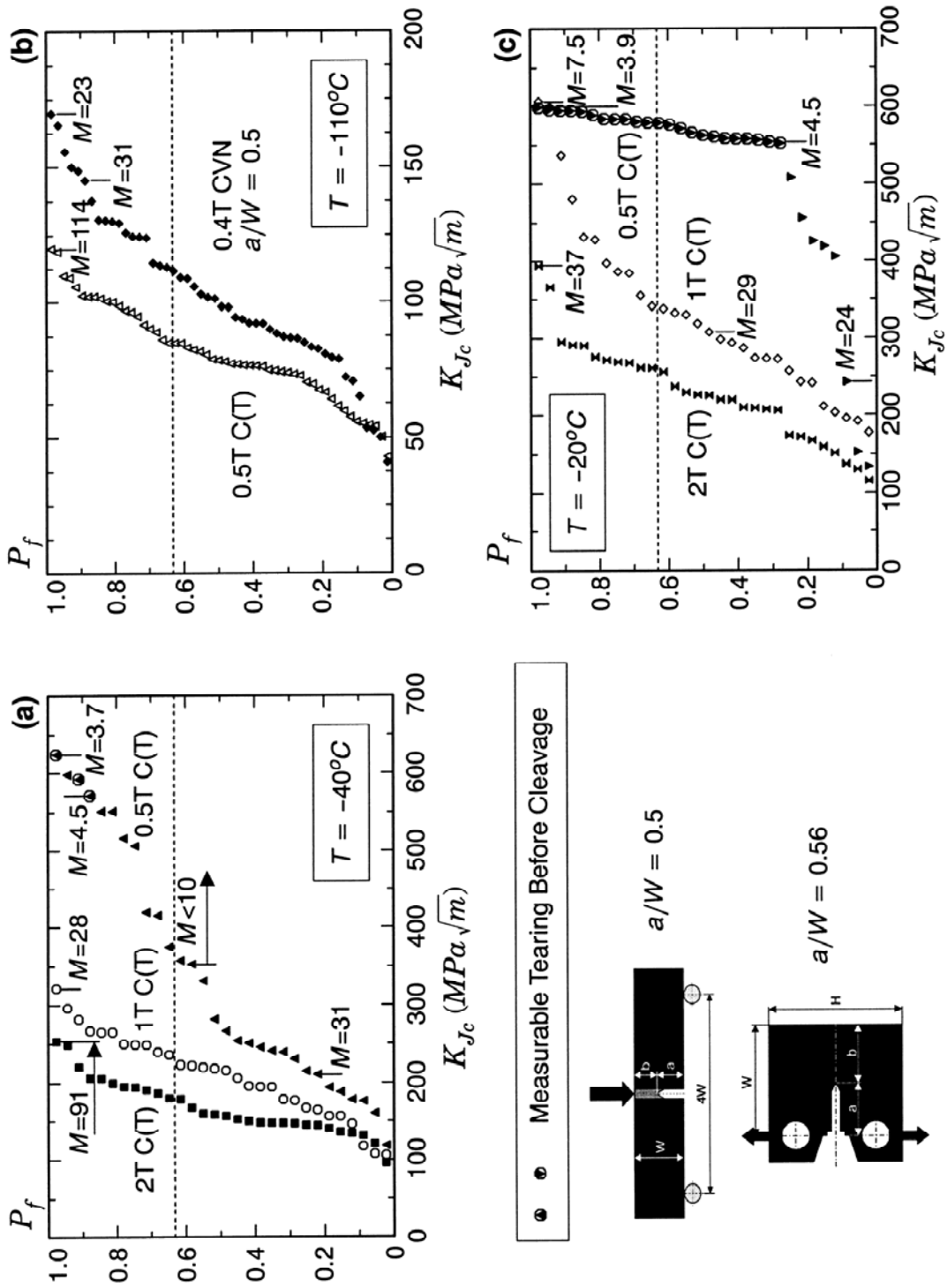


Figure 4. Cumulative (rank) fracture probabilities of raw experimental datasets for the Euro material at (a) $T = -40^\circ C$, (b) $T = -110^\circ C$, (c) $T = -20^\circ C$. These data drive the calibration process for the Weibull stress parameters. The reference temperature $T_0 = -90^\circ C$ from $C(T)$ specimens.

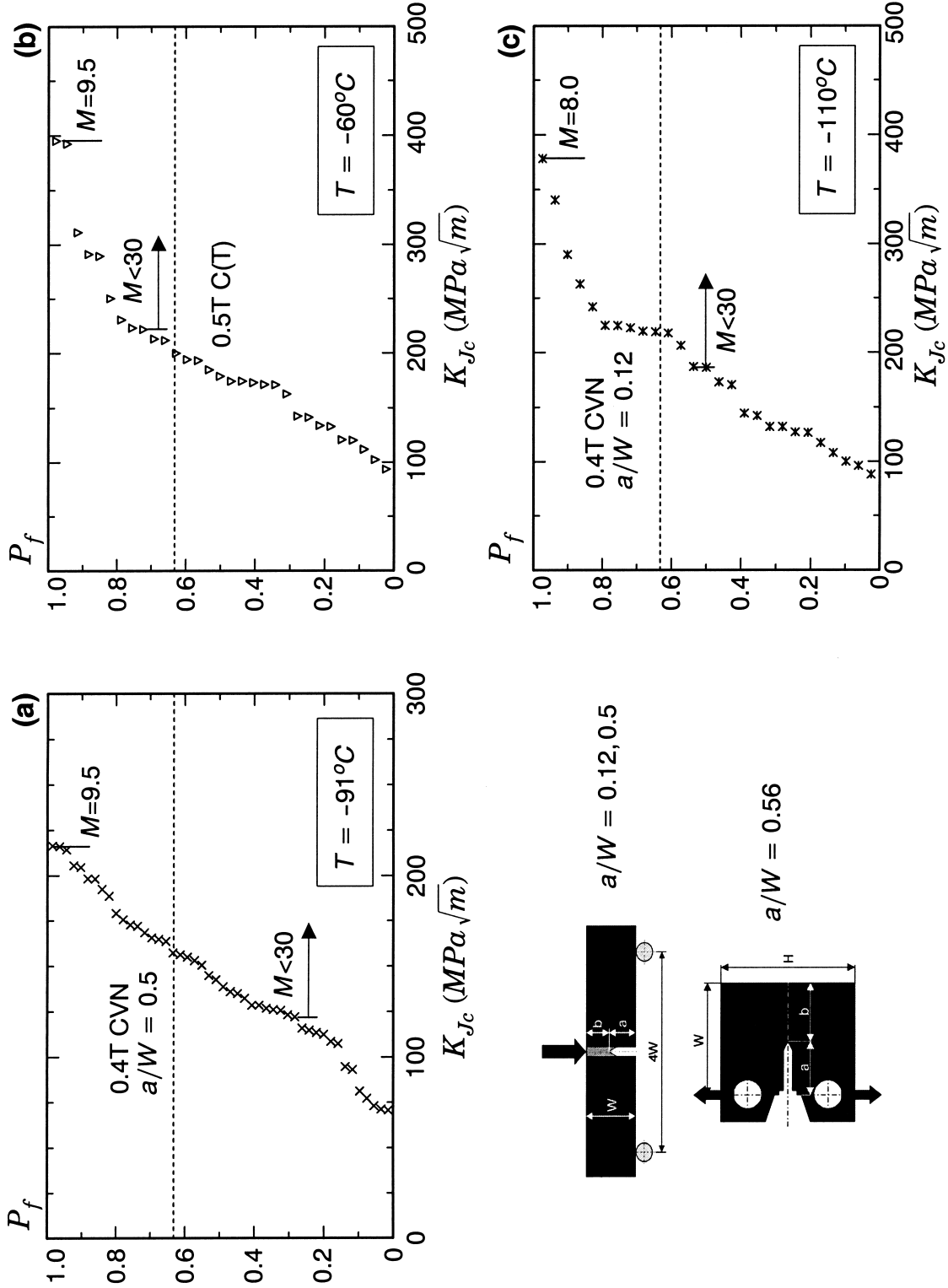


Figure 5. Cumulative (rank) fracture probabilities of raw experimental datasets for the Euro material at (a) $T = -91^\circ C$, (b) $T = -60^\circ C$, (c) $T = -110^\circ C$. These data drive checking of the Weibull stress parameters calibrated using other datasets. The reference temperature $T_0 = -90^\circ C$ from C(T) specimens.

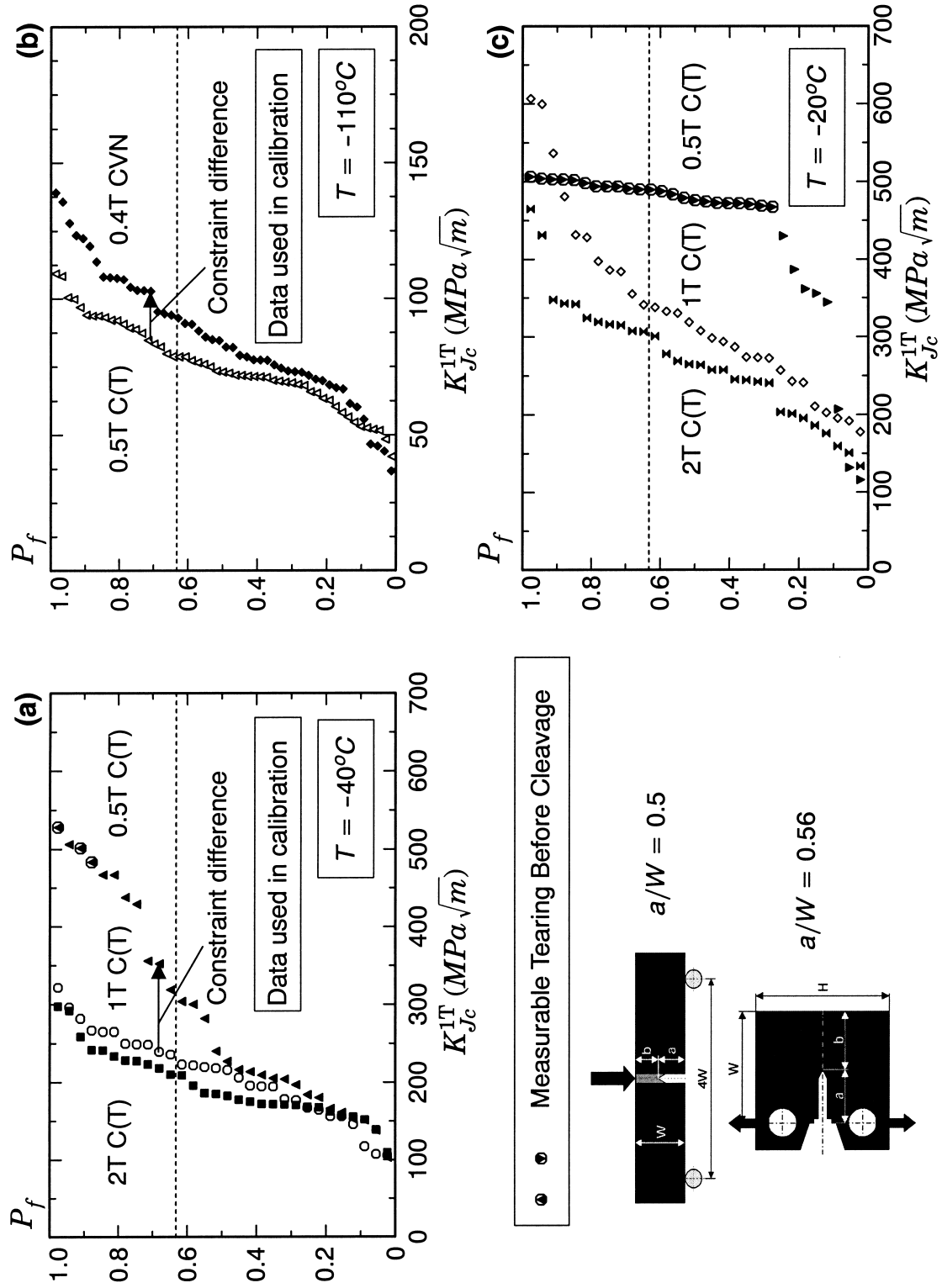


Figure 6. Cumulative (rank) fracture probabilities of experimental datasets for the Euro material crack-front length adjusted to 1T using E1921 procedure at (a) $T = -40^\circ\text{C}$, (b) $T = -110^\circ\text{C}$, (c) $T = -20^\circ\text{C}$. The reference temperature $T_0 = -90^\circ\text{C}$ from C(T) specimens.

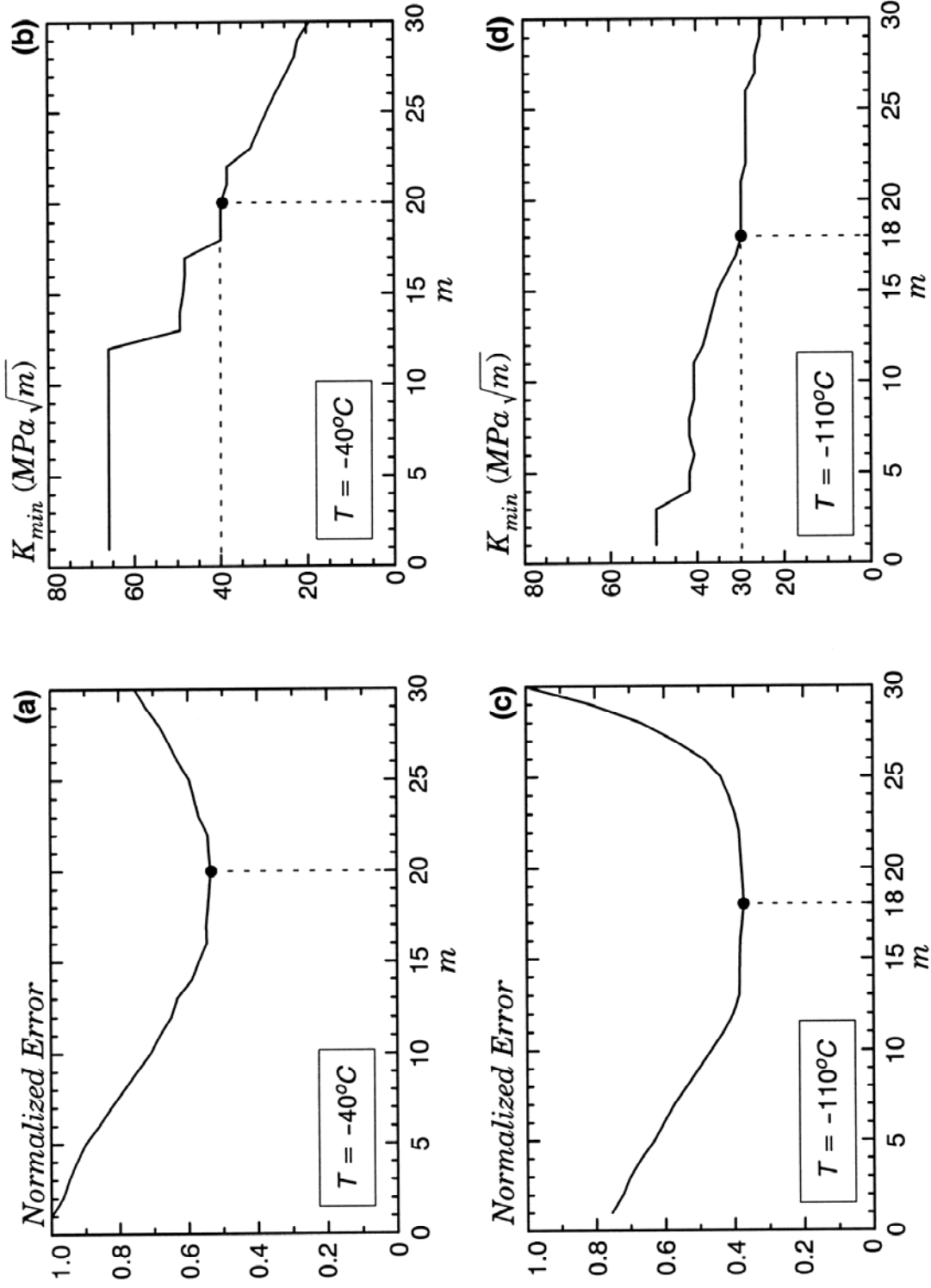


Figure 7. Calibration of Weibull stress parameters for the Euro-material at $T = -40^{\circ}\text{C}$ and $T = -110^{\circ}\text{C}$. Normalized values of error function over range of m -values (a,c); corresponding K_{min} values that lead to minimum error values for each m -value.

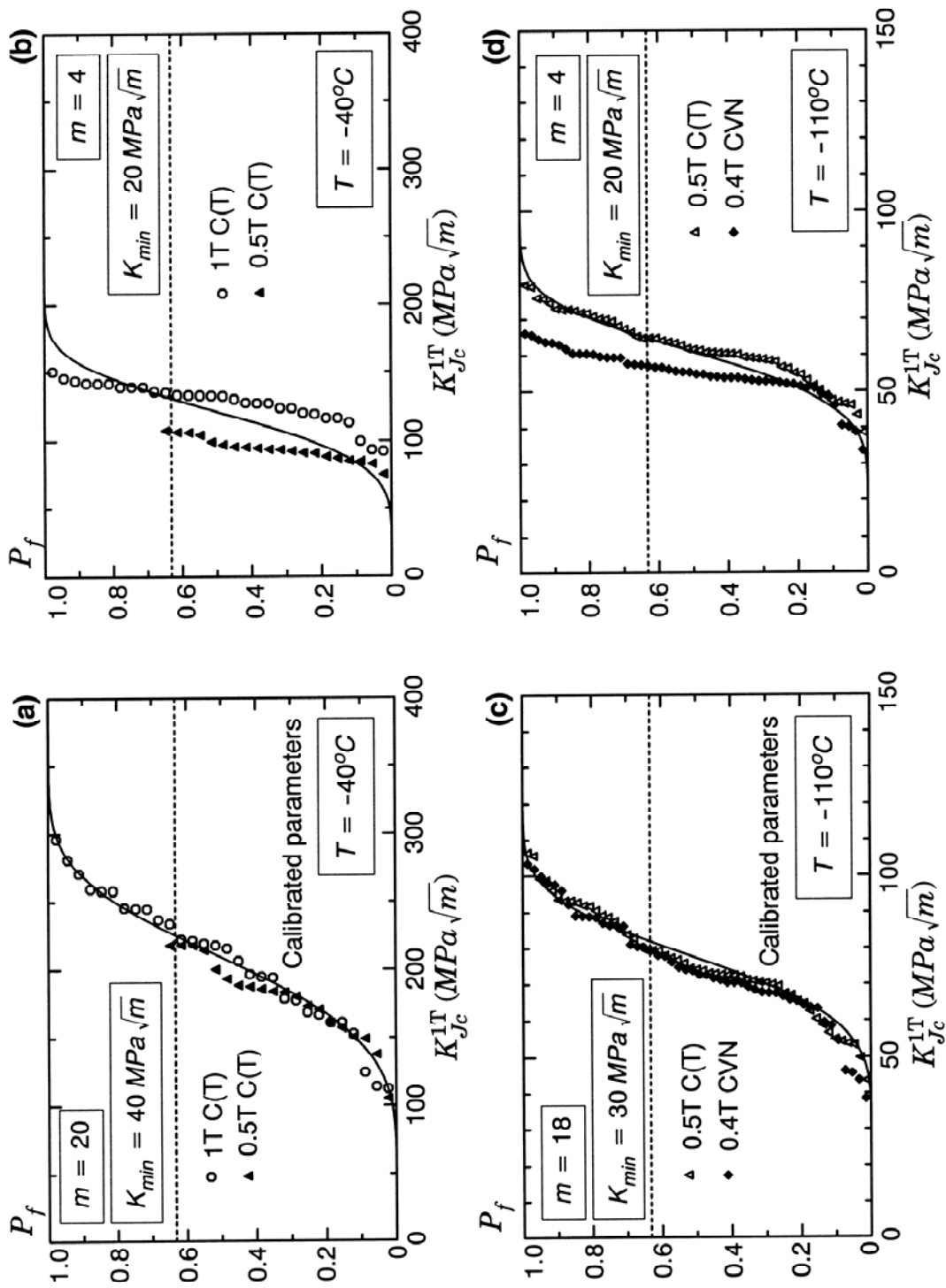


Figure 8. Correction of Euro-material datasets to 1T SSY condition at $T = -40^\circ\text{C}$ and $T = -110^\circ\text{C}$. Using calibrated values of (m, K_{min}) in (a,c); using other values of (m, K_{min}) to illustrate errors of using non-calibrated values.

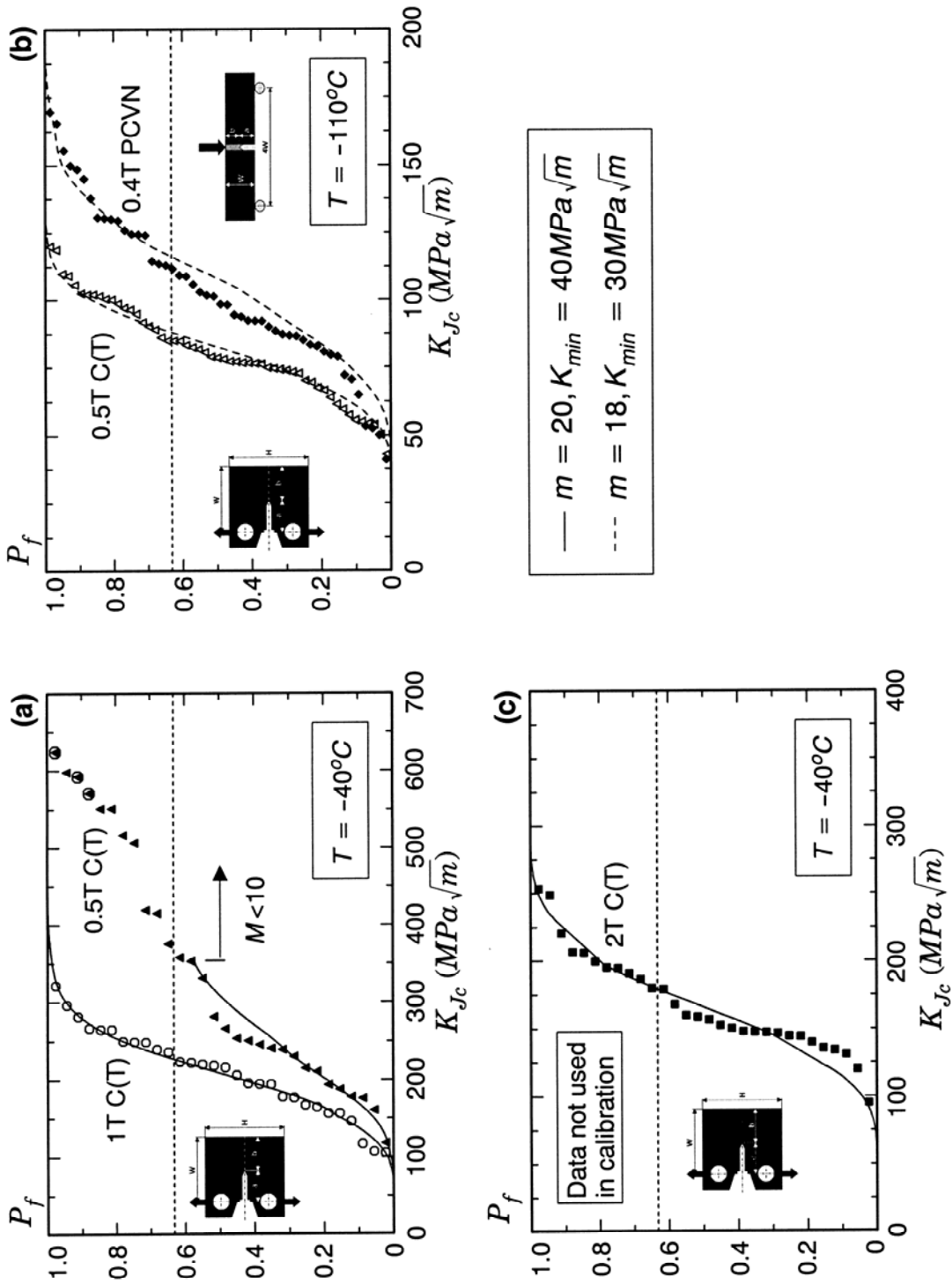


Figure 9. Predicted fracture probabilities of Euro-material using calibrated Weibull stress parameters: (a) $T = -40^{\circ}\text{C}$ data used in calibration, (b) $T = -110^{\circ}\text{C}$ data used in calibration and (c) $T = -40^{\circ}\text{C}$ data not used in calibration.

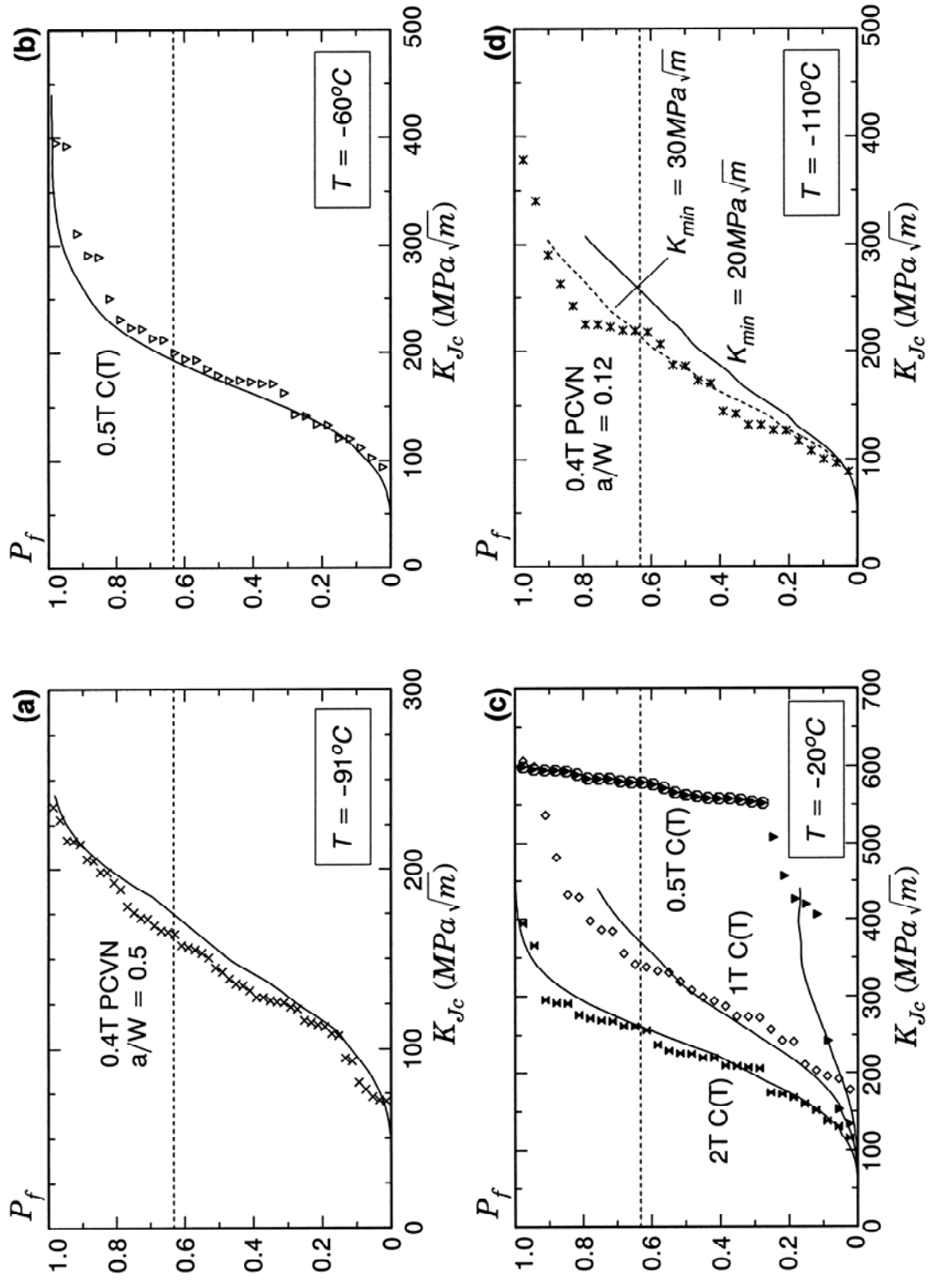
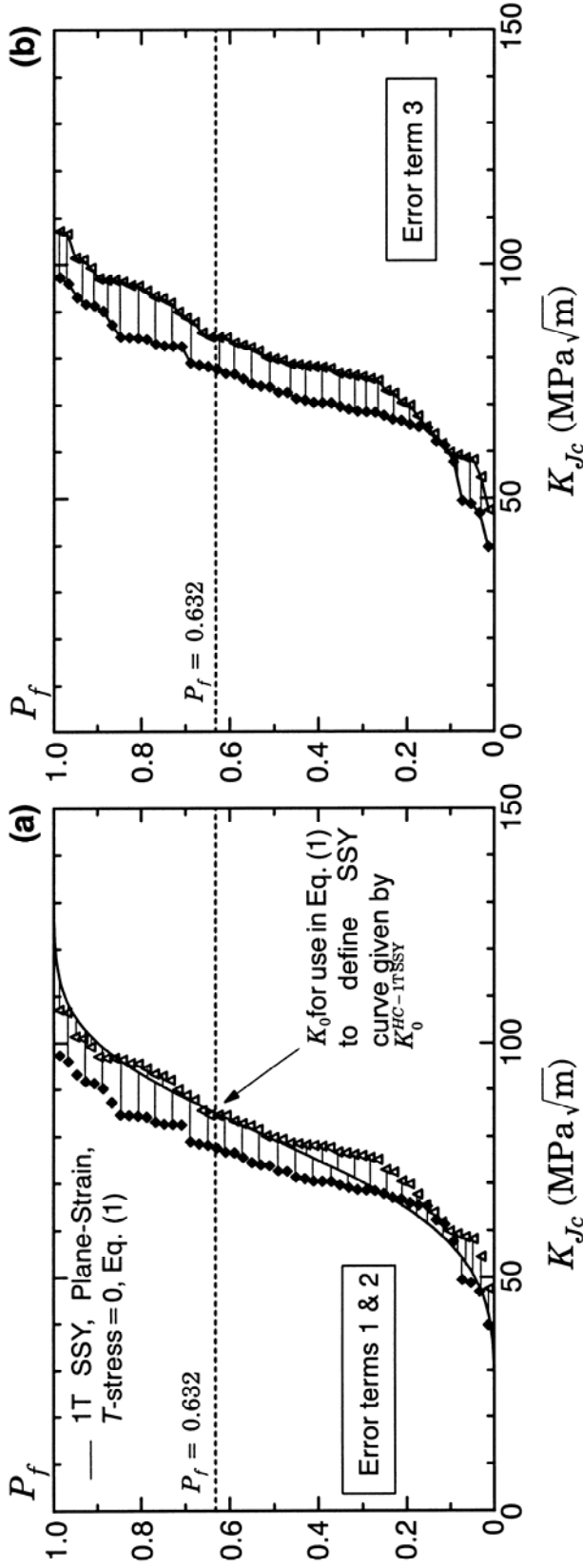


Figure 10. Predicted fracture probabilities for Euro-material specimens not used in any calibrations. Weibull modulus fixed at $m = 20$, $K_{min} = 20 \text{ MPa} \cdot \text{m}^{1/2}$ with temperature dependent σ_{ti} based on the Master Curve.
 (a) $T = -91^\circ\text{C}$, (b) $T = -60^\circ\text{C}$, (c) $T = -20^\circ\text{C}$ and (d) $T = -110^\circ\text{C}$.



- ◆ Low constraint toughness data corrected to 1T-SSY
- △ High constraint toughness data corrected to 1T-SSY

$$(a) \sum_{i=1}^{n_{HC}} |K_{Jc(i)}^{HC-1TSSY} - K_{Jc(i)}^{1TSSY}| WF_{(i)} + \sum_{i=1}^{n_{LC}} |K_{Jc(i)}^{LC-1TSSY} - K_{Jc(i)}^{1TSSY}| WF_{(i)}$$

$$(b) \sum_{i=1}^{\min(n_{HC}, n_{LC})} |K_{Jc(i)}^{HC-1TSSY} - K_{Jc(i)}^{LC-1TSSY}| WF_{(i)}$$

Figure A1. Illustration of contributions to the error measure for calibration of the Weibull stress parameters. (a) difference between experimental data scaled to 1T-SSY and calculated failure probability using 3-parameter form of E1921; (b) difference between low and high constraint experimental data scaled to 1T-SSY.

Table 1. Characteristic parameters of three parameter Weibull stress model for the Euro-material.

$T = - 40^{\circ} C$		
<i>Configuration</i>	σ_u , MPa	σ_{w-min} , MPa
0.5T C(T)	1212	846
1T C(T)	1219	875
2T C(T)	1276	898
1T SSY	1212	844
$m = 20, \bar{C}^{1/m} = 492.36556$ (MPa, m); = 60.52524 (ksi, in)		
$T = - 110^{\circ} C$		
<i>Configuration</i>	σ_u , MPa	σ_{w-min} , MPa
0.5T C(T)	1034	814
0.4T PCVN	1020	781
1T SSY	1097	869
$m = 18, \bar{C}^{1/m} = 477.61145$ (MPa, m); = 57.44222 (ksi, in)		